

## Article

# New Amino Acid Schiff Bases as Anticancer Agents via Potential Mitochondrial Complex I-Associated Hexokinase Inhibition and Targeting AMP-Protein Kinases/mTOR Signaling Pathway

Ahmed A. Noser <sup>1</sup>, Aboubakr H. Abdelmonsef <sup>2,\*</sup>, Mohamed El-Naggar <sup>3</sup> and Maha M. Salem <sup>4</sup>

<sup>1</sup> Organic Chemistry Division, Chemistry Department, Faculty of Science, Tanta University, Tanta 31527, Egypt; ahmed.nosir@science.tanta.edu.eg

<sup>2</sup> Chemistry Department, Faculty of Science, South Valley University, Qena 83523, Egypt

<sup>3</sup> Chemistry Department, Faculty of Sciences, University of Sharjah, Sharjah 27272, United Arab Emirates; melnagrr@sharjah.ac.ae

<sup>4</sup> Biochemistry Division, Chemistry Department, Faculty of Science, Tanta University, Tanta 31527, Egypt; maha\_salem@science.tanta.edu.eg

\* Correspondence: aboubakr.ahmed@sci.svu.edu.eg; Tel.: +20-10-989-65494



**Citation:** Noser, A.A.; Abdelmonsef, A.H.; El-Naggar, M.; Salem, M.M. New Amino Acid Schiff Bases as Anticancer Agents via Potential Mitochondrial Complex I-Associated Hexokinase Inhibition and Targeting AMP-Protein Kinases/mTOR Signaling Pathway. *Molecules* **2021**, *26*, 5332. <https://doi.org/10.3390/molecules26175332>

Academic Editor: María Ángeles Castro

Received: 10 August 2021

Accepted: 31 August 2021

Published: 2 September 2021

**Publisher's Note:** MDPI stays neutral with regard to jurisdictional claims in published maps and institutional affiliations.



**Copyright:** © 2021 by the authors. Licensee MDPI, Basel, Switzerland. This article is an open access article distributed under the terms and conditions of the Creative Commons Attribution (CC BY) license (<https://creativecommons.org/licenses/by/4.0/>).

**Abstract:** Two series of novel amino acid Schiff base ligands containing heterocyclic moieties, such as quinazolinone **3–11** and indole **12–20** were successfully synthesized and confirmed by spectroscopic techniques and elemental analysis. Furthermore, all compounds were investigated in silico for their ability to inhibit mitochondrial NADH: ubiquinone oxidoreductase (complex I) by targeting the AMPK/mTOR signaling pathway and inhibiting hexokinase, a key glycolytic enzyme to prevent the Warburg effect in cancer cells. This inhibitory pathway may be an effective strategy to cause cancer cell death due to an insufficient amount of ATP. Our results revealed that, out of 18 compounds, two (**11** and **20**) were top-ranked as they exhibited the highest binding energies of  $-8.8$ ,  $-13.0$ ,  $-7.9$ , and  $-10.0$  kcal/mol in the docking analysis, so they were then selected for in vitro assessment. Compound **11** promoted the best cytotoxic effect on MCF-7 with  $IC_{50} = 64.05 \pm 0.14$   $\mu\text{g}/\text{mL}$  ( $0.135$  mM) while compound **20** exhibited the best cytotoxic effect on MDA-231 with  $IC_{50} = 46.29 \pm 0.09$   $\mu\text{g}/\text{mL}$  ( $0.166$  mM). Compounds **11** and **20** showed significant activation of AMPK protein and oxidative stress, which led to elevated expression of p53 and Bax, reduced Bcl-2 expression, and caused cell cycle arrest at the sub- $G_0/G_1$  phase. Moreover, compounds **11** and **20** showed significant inhibition of the mTOR protein, which led to the activation of aerobic glycolysis for survival. This alternative pathway was also blocked as compounds **11** and **20** showed significant inhibitory effects on the hexokinase enzyme. These findings demonstrate that compounds **11** and **20** obeyed Lipinski's rule of five and could be used as privileged scaffolds for cancer therapy via their potential inhibition of mitochondrial complex I-associated hexokinase.

**Keywords:** cancer; hexokinase; NADH: ubiquinone oxidoreductase; docking study; cytotoxic activity

## 1. Introduction

Cancer represents a major global public health problem and is still associated with significant mortality [1]. Given the widespread occurrence of cancer drug resistance and a lack of sensitivity of tumor cells to such drugs, there is an urgent need for novel, effective, and less harmful antitumor agents that act by inhibiting specific metabolic target proteins [2]. Particularly important in this context is the synthesis of bioenergetic drugs that not only impact ATP production but also disrupt the biosynthetic pathway that relies on precursor metabolites found in the generation of ATP as required for cancer cell proliferation [3]. NADH: ubiquinone oxidoreductase (complex I) is the entry point of reduced NADH into the electron transport chain. Direct inhibition of complex I in

cancer cells decreases the proton gradient and mitochondrial oxygen consumption rate [4], diminishes tricarboxylic acid cycle (TCA) activity and metabolites [4,5], and leads to decreased cellular ATP levels [6–8].

The inhibition of mitochondrial respiration and ATP production results in a compensatory increase in glycolysis through the Warburg effect (aerobic glycolysis) to restore cellular ATP levels required for the survival of cancer cells. The inhibition of hexokinase (ATP: D-hexose 6-phosphotransferase), a key enzyme that catalyzes the first step in the glycolysis pathway, prevents the rerouting of metabolic flux and leads to the depletion of cellular ATP. When ATP cannot meet the requirements of cancer cells and oxidative stress occurs, which promotes reactive oxygen species (ROS) generation, AMP-protein kinases (AMPK) become activated, and the mitochondrial membrane potential becomes dysfunctional [8–10]. Phosphorylation and activation of AMPK leads to the activation of p53 and Bax, arrests cell cycle progression, inactivates mammalian target of rapamycin (mTOR), decreases protein synthesis, and decreases the transcription of gluconeogenic genes.

Many efforts have been made to synthesize novel effective and selective anticancer drugs for complex I and hexokinase inhibition as they can worsen the cellular energy status, leading to a global decrease in ATP-consuming processes, and also induce oxidative stress. In proliferating cells, this can elicit a cytostatic state that is associated with reduced proliferation, explaining some clinical observations of decreased progression of cancer cell growth. Cancer cells that cannot eventually compensate for this reduced energy status and are affected by ROS generation may undergo apoptosis [11,12].

The Schiff base compounds (imines) containing heterocyclic systems, such as quinazolinone and indole nuclei, azomethine linkages, and phenyl rings, have attracted particular attention due to their potential applications in medicinal and pharmaceutical chemistry [13,14].

Quinazolinone and indole are good pharmacophoric scaffolds found in many biologically active compounds ranging from natural products to synthetic pharmaceutical drugs. These compounds are known to be associated with antimalarial, antimicrobial, anticonvulsant, and anticancer effects [15–19].

Given the importance of imines (Schiff bases) in the medicinal field and the continuous efforts by our group to develop novel anticancer scaffolds [2,20–28], the aim of this study was first to design and synthesize novel quinazolinone and indole amino acid Schiff bases. The synthesized compounds were then subjected to computer-based docking studies to investigate their binding modes of interaction with the active site of the target enzymes. In addition, they underwent *in silico* physicochemical and pharmacokinetic investigations to predict their absorption, distribution, metabolism, excretion, and toxicity (ADMET) properties, as well as analysis of the structure–activity relationship (SAR) of the compounds. Finally, the compounds were examined *in vitro* for inhibitory activities against mitochondrial NADH: ubiquinone oxidoreductase (complex I) by targeting the AMPK/mTOR signaling pathway and inhibiting hexokinase, a key glycolytic enzyme, to prevent the Warburg effect in cancer cells.

## 2. Materials and Methods

### 2.1. Chemicals and Drugs

Anthranilic acid, benzoyl chloride, p-aminoacetophenone, indol-3-carboxaldehyde, pyridine, triethylamine, glycine, phenylglycine, alanine, phenylalanine, serine, tyrosine, leucine, lysine, asparagine, thiobarbituric acid, trichloroacetic acid (TCA), reduced glutathione (GSH), and sodium pyrophosphate were purchased from Sigma-Aldrich Chemical Co. (St. Louis, MO, USA). Tamoxifen was purchased from EIMC United Pharmaceuticals (Cairo, Egypt).

#### 2.1.1. General Information

Reactions were monitored by TLC performed on pre-coated plates Merck Kieselgel 60 F254 (EMD Millipore Corporation, Billerica, MA, USA). Infrared spectra were recorded

at the central laboratory of Tanta University using a PerkinElmer 1420 spectrophotometer (Waltham, MA, USA). The spectra were obtained using the KBr disc technique. The samples were dried in an oven and then mounted on a sample holder with a large cavity. Melting points were determined by the open capillary method using the Gallenkamp melting point and are reported uncorrected. The elemental analyses of compounds were performed at the microanalytical center of Cairo University using a PerkinElmer 240 CHN Elemental analyzer (Waltham, MA, USA).  $^1\text{H-NMR}$  and  $^{13}\text{C-NMR}$  spectra were collected at a resonance frequency of 400 MHz at Kafr El-Sheikh University. NMR spectra were obtained on a Bruker AMC instrument (Bruker Biosciences Corporation, Billerica, MA, USA) operating at 400 MHz using dimethyl sulfoxide (DMSO) as a solvent and tetramethylsilane as an internal standard. The chemical shifts for  $^1\text{H-NMR}$  are reported in ppm from tetramethylsilane (0 ppm) or referenced to the solvent (DMSO- $d_6$ ,  $\delta$  2.50). Chemical shifts ( $\delta$ ) for  $^{13}\text{C-NMR}$  spectra are referenced to the signals for residual deuterated solvents (DMSO- $d_6$ , 37.5). Multiplicities are reported using the following abbreviations: s (singlet), d (doublet), t (triplet), and m (multiplet).

#### 2.1.2. Synthesis of 2-Phenyl-4*H*-benzo[d][1,3] Oxazin-4-one (1)

Compound 1 was prepared as described by Tiwary [29] with an 86% yield.

#### 2.1.3. Synthesis of 3-(4-Acetylphenyl)-2-phenylquinazolin-4(3*H*)-one (2)

Compound 2 was prepared as described by Patel [30] with an 82% yield.

#### 2.1.4. Synthesis of Amino Acid Schiff Bases

##### General method:

The Schiff bases 3–20 were synthesized by the condensation of a carbonyl compound (3-(4-acetylphenyl)-2-phenylquinazolin-4(3*H*)-one and/or indol-3-carboxaldehyde) (1 mmol) and derivatives of amino acids (1 mmol) after stirring for 30 min with  $\text{Et}_3\text{N}$  dissolved in dry ethanol (10 mL). The resulting reaction mixture was stirred and refluxed for 9 h (TLC control) and then allowed to cool overnight. The precipitated Schiff bases were filtered, washed with cold ethanol several times, and dried at room temperature. The solid products were then recrystallized with ethanol [31].

#### 2-(1-(4-(4-oxo-2-Phenylquinazolin-3(4*H*)-yl) phenyl) ethylideneamino) Acetic Acid (3)

Yield 82%; mp 146 °C;  $^1\text{H-NMR}$  (400 MHz, DMSO- $d_6$ )  $\delta$  (ppm): 11.00 (s, 1H, COOH), 7.08–7.95 (m, 13H, Ar-H), 4.49 (s, 2H,  $\text{CH}_2$ ), 0.96 (s, 3H,  $\text{CH}_3$ );  $^{13}\text{C-NMR}$  (400 MHz, DMSO- $d_6$ )  $\delta$  (ppm): 171.60, 164.60, 164.20, 161.10, 151.50, 135.90, 135.30, 133.70, 130.40, 130.00, 129.60, 129.10, 128.90, 127.60, 126.30, 122.60, 121.90, 121.10, 54.70, 22.30; IR (KBr)  $\nu$ : 3027 (arom. CH stretch), 2953 (aliph. CH stretch), 2900 (OH), 1715 (CO), 1610–1655 (C=N); Anal. Calcd for  $\text{C}_{24}\text{H}_{19}\text{N}_3\text{O}_3$  (397.43): C, 72.53%; H, 4.82%; O, 12.08%; N, 10.57%. Found: C, 72.26%; H, 4.61%; N, 10.36%.

#### 2-(1-(4-(4-oxo-2-Phenylquinazolin-3(4*H*)-yl) phenyl) ethylideneamino) Propionic Acid (4)

Yield 80%; mp 191 °C;  $^1\text{H-NMR}$  (400 MHz, DMSO- $d_6$ )  $\delta$  (ppm): 11.00 (s, 1H, COOH), 7.08–7.95 (m, 13H, Ar-H), 4.18 (m, 1H, CH), 1.42 (d, 3H,  $\text{CH}_3$ ), 0.96 (s, 3H,  $\text{CH}_3$ );  $^{13}\text{C-NMR}$  (400 MHz, DMSO- $d_6$ )  $\delta$  (ppm): 177.70, 164.60, 164.20, 161.10, 151.50, 135.90, 135.30, 133.70, 130.40, 130.00, 129.60, 129.10, 128.90, 127.60, 126.30, 122.60, 121.90, 121.10, 62.80, 22.60, 18.20; IR (KBr)  $\nu$ : 3027 (arom. CH stretch), 2956 (aliph. CH stretch), 2915 (OH), 1725 (CO), 1615–1659 (C=N); Anal. Calcd for  $\text{C}_{25}\text{H}_{21}\text{N}_3\text{O}_3$  (411.45): C, 72.98%; H, 5.14%; O, 11.67%; N, 10.21%. Found: C, 72.36%; H, 4.91%; N, 10.32%.

#### 2-(1-(4-(4-oxo-2-Phenylquinazolin-3(4*H*)-yl) phenyl) ethylidene amino)-3-phenyl Propionic Acid (5)

Yield 84%; mp 165 °C;  $^1\text{H-NMR}$  (400 MHz, DMSO- $d_6$ )  $\delta$  (ppm): 11.00 (s, 1H, COOH), 6.81–7.95 (m, 18H, Ar-H), 4.39 (t, 1H, CH), 3.29 (d, 2H,  $\text{CH}_2$ ), 0.96 (s, 3H,  $\text{CH}_3$ );  $^{13}\text{C-NMR}$

(400 MHz, DMSO- $d_6$ )  $\delta$  (ppm): 177.70, 164.60, 164.20, 161.10, 151.50, 139.70, 135.90, 135.30, 133.70, 130.40, 130.00, 129.60, 129.10, 128.90, 128.00, 127.60, 126.30, 126.20, 122.60, 121.90, 121.10, 66.80, 38.40, 22.60; IR (KBr)  $\nu$ : 3037 (arom. CH stretch), 2956 (aliph. CH stretch), 1715 (CO), 2912 (OH), 1612–1657 (C=N); Anal. Calcd for  $C_{31}H_{25}N_3O_3$  (487.55): C, 76.37%; H, 5.17%; O, 9.84%; N, 8.62%. Found: C, 76.11%; H, 4.99%; N, 8.46%.

3-Hydroxy-2-(1-(4-(4-oxo-2-phenylquinazolin-3(4H)-yl) phenyl) ethylidene amino) Propionic Acid (6)

Yield 80%; mp 184 °C;  $^1H$ -NMR (400 MHz, DMSO- $d_6$ )  $\delta$  (ppm): 11.00 (s, 1H, COOH), 7.08–7.95 (m, 13H, Ar-H), 4.25 (d, 2H,  $CH_2$ ), 4.09 (t, 1H, CH), 2.00 (s, 1H, OH), 0.96 (s, 3H,  $CH_3$ );  $^{13}C$ -NMR (400 MHz, DMSO- $d_6$ )  $\delta$  (ppm): 177.70, 164.60, 164.20, 161.10, 151.50, 135.90, 135.30, 133.70, 130.40, 130.00, 129.60, 129.10, 128.90, 127.60, 126.30, 122.60, 121.90, 121.10, 66.20, 64.00, 22.60; IR (KBr)  $\nu$ : 3250 ( $CH_2$ -OH), 3027 (arom. CH stretch), 2953 (aliph. CH stretch), 2900 (carboxylic-OH), 1715 (CO), 1610–1655 (C=N); Anal. Calcd for  $C_{25}H_{21}N_3O_4$  (427.45): C, 70.25%; H, 4.95%; O, 14.97%; N, 9.83%. Found: C, 69.46%; H, 4.76%; N, 9.66%.

3-(4-Hydroxyphenyl)-2-(1-(4-(4-oxo-2-phenylquinazolin-3(4H)-yl) phenyl) ethylidene amino) Propionic Acid (7)

Yield 86%; mp 150 °C;  $^1H$  NMR (400 MHz, DMSO- $d_6$ )  $\delta$  (ppm): 11.00 (s, 1H, COOH), 7.08–7.95 (m, 13H, Ar-H), 6.61–6.75 (m, 4H, Ar-H), 5.00 (s, 1H, OH), 4.39 (t, 1H, CH), 3.22 (d, 2H,  $CH_2$ ), 0.96 (s, 3H,  $CH_3$ );  $^{13}C$  NMR (400 MHz, DMSO- $d_6$ )  $\delta$  (ppm): 178.10, 164.80, 164.20, 161.10, 157.50, 151.50, 135.90, 135.30, 133.70, 131.30, 130.40, 130.00, 129.60, 129.10, 128.90, 127.60, 126.30, 122.60, 121.90, 121.10, 116.50, 66.80, 38.60, 16.60; IR (KBr)  $\nu$ : 3290 (arom-OH), 3027 (arom. CH stretch), 2953 (aliph. CH stretch), 2900 (carboxylic-OH), 1715 (CO), 1610–1655 (C=N); Anal. Calcd for  $C_{31}H_{25}N_3O_4$  (503.55): C, 73.94%; H, 5.00%; O, 12.71%; N, 8.34%. Found: C, 73.16%; H, 4.83%; N, 8.16%.

4-Methyl-2-(1-(4-(4-oxo-2-phenylquinazolin-3(4H)-yl) phenyl) ethylideneamino) Pentanoic Acid (8)

Yield 84%; mp 154 °C;  $^1H$ -NMR (400 MHz, DMSO- $d_6$ )  $\delta$  (ppm): 11.00 (s, 1H, COOH), 7.08–7.95 (m, 13H, Ar-H), 4.00 (t, 1H, CH), 1.85 (t, 2H,  $CH_2$ ), 1.83 (m, 1H, CH), 1.15 (d, 6H, 2 $CH_3$ ), 0.96 (s, 3H,  $CH_3$ );  $^{13}C$ -NMR (400 MHz, DMSO- $d_6$ )  $\delta$  (ppm): 177.70, 164.80, 164.20, 161.10, 151.50, 135.90, 135.30, 133.70, 130.40, 130.00, 129.60, 129.10, 128.90, 127.60, 126.30, 122.60, 121.90, 121.10, 56.90, 23.50, 23.20, 23.10, 16.60; IR (KBr)  $\nu$ : 3027 (arom. CH stretch), 2953 (aliph. CH stretch), 2900 (OH), 1715 (CO), 1610–1655 (C=N); Anal. Calcd for  $C_{28}H_{27}N_3O_3$  (453.53): C, 74.15%; H, 6.00%; O, 10.58%; N, 9.27%. Found: C, 73.26%; H, 5.81%; N, 8.36%.

6-Amino-2-(1-(4-(4-oxo-2-phenylquinazolin-3(4H)-yl) phenyl) ethylideneamino) Hexanoic Acid (9)

Yield 80%; mp 193 °C;  $^1H$ -NMR (400 MHz, DMSO- $d_6$ )  $\delta$  (ppm): 11.00 (s, 1H, COOH), 7.08–7.95 (m, 13H, Ar-H), 4.00 (t, 1H, CH), 2.71 (t, 2H, N- $CH_2$ ), 2.00 (s, 2H,  $NH_2$ ), 1.88 (m, 2H, CH- $CH_2$ ), 1.29–1.38 (m, 4H, 2 $CH_2$ ), 0.96 (s, 3H,  $CH_3$ );  $^{13}C$ -NMR (400 MHz, DMSO- $d_6$ )  $\delta$  (ppm): 177.70, 164.80, 164.20, 161.10, 151.50, 135.90, 135.30, 133.70, 130.40, 130.00, 129.60, 129.10, 128.90, 127.60, 126.30, 122.60, 121.90, 121.10, 59.70, 42.30, 38.30, 32.70, 16.60, 12.80; IR (KBr)  $\nu$ : 3390 ( $NH_2$ ), 3027 (arom. CH stretch), 2953 (aliph. CH stretch), 2900 (OH), 1715 (CO), 1610–1655 (C=N); Anal. Calcd for  $C_{28}H_{28}N_4O_3$  (468.55): C, 71.78%; H, 6.02%; O, 10.24%; N, 11.96%. Found: C, 71.16%; H, 5.81%; N, 11.46%.

4-Amino-4-oxo-2-(1-(4-(4-oxo-2-phenylquinazolin-3(4H)-yl) phenyl) ethylidene amino) Butanoic Acid (10)

Yield 87%; mp 140 °C;  $^1H$ -NMR (400 MHz, DMSO- $d_6$ )  $\delta$  (ppm): 11.00 (s, 1H, COOH), 7.08–7.95 (m, 13H, Ar-H), 6.00 (s, 2H,  $NH_2$ ), 4.23 (t, 1H, CH), 2.64–2.77 (d, 2H,  $CH_2$ ), 0.96 (s, 3H,  $CH_3$ );  $^{13}C$ -NMR (400 MHz, DMSO- $d_6$ )  $\delta$  (ppm): 177.70, 174.80, 164.80, 164.20, 161.10, 151.50, 135.90, 135.30, 133.70, 130.40, 130.00, 129.60, 129.10, 128.90, 127.60, 126.30, 122.60,

121.90, 121.10, 56.50, 37.50, 16.60; IR (KBr)  $\nu$ : 3390 (NH<sub>2</sub>), 3027 (arom. CH stretch), 2953 (aliph. CH stretch), 2900 (OH), 1715 (CO), 1610–1655 (C=N); Anal. Calcd for C<sub>26</sub>H<sub>22</sub>N<sub>4</sub>O<sub>4</sub> (454.48): C, 68.71%; H, 4.88%; O, 14.08%; N, 12.33%. Found: C, 68.14%; H, 4.71%; N, 11.96%.

2-(1-(4-(4-oxo-2-Phenylquinazolin-3(4*H*)-yl) phenyl) ethylideneamino)-2-phenyl Acetic Acid (**11**)

Yield 87%; mp 196 °C; <sup>1</sup>H NMR (400 MHz, DMSO-*d*<sub>6</sub>)  $\delta$  (ppm): 11.00 (s, 1H, COOH), 7.08–7.95 (m, 13H, Ar-H), 6.84–6.95 (m, 5H, Ar-H), 5.32 (s, 1H, CH), 0.96 (s, 3H, CH<sub>3</sub>); <sup>13</sup>C NMR (400 MHz, DMSO-*d*<sub>6</sub>)  $\delta$  (ppm): 178.20, 164.80, 164.20, 161.10, 151.50, 138.70, 135.90, 135.30, 133.70, 130.40, 130.00, 129.60, 129.40, 129.10, 128.90, 127.80, 127.60, 126.30, 122.60, 121.90, 121.10, 64.70, 22.60; IR (KBr)  $\nu$ : 3027 (arom. CH stretch), 2953 (aliph. CH stretch), 2900 (OH), 1715 (CO), 1610–1655 (C=N); Anal. Calcd for C<sub>30</sub>H<sub>23</sub>N<sub>3</sub>O<sub>3</sub> (473.52): C, 76.09%; H, 4.90%; O, 10.14%; N, 8.87%. Found: C, 75.26%; H, 4.74%; N, 8.16%.

2-((1*H*-Indol-3-yl) methyleneamino) Acetic Acid (**12**)

Yield 92%; mp 175 °C; <sup>1</sup>H-NMR (400 MHz, DMSO-*d*<sub>6</sub>)  $\delta$  (ppm): 11.00 (s, 1H, COOH), 9.50 (s, 1H, NH), 7.50 (s, 1H, CH=N), 7.11–7.58 (m, 5H, Ar-H), 2.31 (s, 2H, CH<sub>2</sub>); <sup>13</sup>C-NMR (400 MHz, DMSO-*d*<sub>6</sub>)  $\delta$  (ppm): 171.60, 161.10, 135.70, 131.00, 126.30, 122.40, 120.30, 119.20, 111.30, 102.20, 55.20; IR (KBr)  $\nu$ : 3027 (arom. CH stretch), 2953 (aliph. CH stretch), 2915 (OH), 1715 (CO), 1610–1655 (C=N); Anal. Calcd for C<sub>11</sub>H<sub>10</sub>N<sub>2</sub>O<sub>2</sub> (202.21): C, 65.34%; H, 4.98%; O, 15.82%; N, 13.85%. Found: C, 65.11%; H, 4.65%; N, 13.24%.

2-((1*H*-Indol-3-yl)methyleneamino) Propionic Acid (**13**)

Yield 87%; mp 120 °C; <sup>1</sup>H-NMR (400 MHz, DMSO-*d*<sub>6</sub>)  $\delta$  (ppm): 11.00 (s, 1H, COOH), 9.50 (s, 1H, NH), 7.50 (s, 1H, CH=N), 7.11–7.58 (m, 5H, Ar-H), 2.65 (m, 1H, CH), 1.11 (d, 3H, CH<sub>3</sub>); <sup>13</sup>C-NMR (400 MHz, DMSO-*d*<sub>6</sub>)  $\delta$  (ppm): 171.60, 161.10, 135.70, 131.00, 126.30, 122.40, 120.30, 119.20, 111.30, 102.20, 55.20; IR (KBr)  $\nu$ : 3037 (arom. CH stretch), 2966 (aliph. CH stretch), 2925 (OH), 1715 (CO), 1615–1649 (C=N); Anal. Calcd for C<sub>12</sub>H<sub>12</sub>N<sub>2</sub>O<sub>2</sub> (216.24): C, 66.65%; H, 5.59%; O, 14.80%; N, 12.96%. Found: C, 66.39%; H, 5.24%; N, 12.64%.

2-((1*H*-Indol-3-yl) methyleneamino)-3-phenylpropionic Acid (**14**)

Yield 89%; mp 180 °C; <sup>1</sup>H-NMR (400 MHz, DMSO-*d*<sub>6</sub>)  $\delta$  (ppm): 11.00 (s, 1H, COOH), 9.50 (s, 1H, NH), 7.50 (s, 1H, CH=N), 7.11–7.81 (m, 10H, Ar-H), 3.11 (d, 2H, CH<sub>2</sub>), 2.89 (t, 1H, CH); <sup>13</sup>C-NMR (400 MHz, DMSO-*d*<sub>6</sub>)  $\delta$  (ppm): 177.70, 161.10, 139.70, 135.70, 131.00, 128.90, 128.00, 126.30, 126.20, 122.40, 120.30, 119.20, 111.30, 102.20, 67.30, 38.30; IR (KBr)  $\nu$ : 3037 (arom. CH stretch), 2956 (aliph. CH stretch), 2923 (OH), 1716 (CO), 1615–1655 (C=N); Anal. Calcd for C<sub>18</sub>H<sub>16</sub>N<sub>2</sub>O<sub>2</sub> (292.33): C, 73.95%; H, 5.52%; O, 10.95%; N, 9.58%. Found: C, 73.21%; H, 5.27%; N, 9.17%.

2-((1*H*-Indol-3-yl) methyleneamino)-3-hydroxy Propionic Acid (**15**)

Yield 91%; mp 163 °C; <sup>1</sup>H-NMR (400 MHz, DMSO-*d*<sub>6</sub>)  $\delta$  (ppm): 11.00 (s, 1H, COOH), 9.50 (s, 1H, NH), 7.50 (s, 1H, CH=N), 7.11–7.58 (m, 5H, Ar-H), 3.90 (d, 2H, CH<sub>2</sub>), 2.65 (t, 1H, CH), 2.00 (s, 1H, OH); <sup>13</sup>C-NMR (400 MHz, DMSO-*d*<sub>6</sub>)  $\delta$  (ppm): 177.70, 161.10, 135.70, 131.00, 126.30, 122.40, 120.30, 119.20, 111.30, 102.20, 66.70, 63.70; IR (KBr)  $\nu$ : 3260 (CH<sub>2</sub>-OH), 3027 (arom. CH stretch), 2953 (aliph. CH stretch), 2900 (carboxylic-OH), 1715 (CO), 1610–1655 (C=N); Anal. Calcd for C<sub>12</sub>H<sub>12</sub>N<sub>2</sub>O<sub>3</sub> (232.24): C, 62.06%; H, 5.21%; O, 20.67%; N, 12.06%. Found: C, 61.72%; H, 4.86%; N, 11.66%.

2-((1*H*-Indol-3-yl) methyleneamino)-3-(4-hydroxyphenyl) Propionic Acid (**16**)

Yield 94%; mp 203 °C; <sup>1</sup>H NMR (400 MHz, DMSO-*d*<sub>6</sub>)  $\delta$  (ppm): 11.00 (s, 1H, COOH), 9.50 (s, 1H, NH), 7.50 (s, 1H, CH=N), 7.11–7.41 (m, 5H, Ar-H), 6.65–6.95 (m, 4H, Ar-H), 5.00 (s, 1H, OH), 3.71 (t, 1H, CH), 2.90 (d, 2H, CH<sub>2</sub>); <sup>13</sup>C NMR (400 MHz, DMSO-*d*<sub>6</sub>)  $\delta$  (ppm): 177.70, 161.10, 159.90, 135.70, 132.30, 131.00, 129.40, 126.30, 122.40, 120.30, 119.20, 116.00, 111.30, 102.20, 73.30, 38.30; IR (KBr)  $\nu$ : 3290

(arom-OH), 3027 (arom. CH stretch), 2953 (aliph. CH stretch), 2900 (carboxylic-OH), 1715 (CO), 1610–1655 (C=N); Anal. Calcd for  $C_{18}H_{16}N_2O_3$  (308.33): C, 70.12%; H, 5.23%; O, 15.57%; N, 9.09%. Found: C, 69.76%; H, 4.99%; N, 8.76%.

#### 2-((1*H*-Indol-3-yl) methyleneamino)-4-methylpentanoic Acid (17)

Yield 94%; mp 207 °C;  $^1H$ -NMR (400 MHz, DMSO- $d_6$ )  $\delta$  (ppm): 11.00 (s, 1H, COOH), 9.50 (s, 1H, NH), 7.50 (s, 1H, CH=N), 7.11–7.55 (m, 5H, Ar-H), 2.40 (t, 1H, CH), 1.83 (m, 1H, CH), 1.55 (t, 2H, CH<sub>2</sub>), 1.00 (d, 6H, 2CH<sub>3</sub>);  $^{13}C$ -NMR (400 MHz, DMSO- $d_6$ )  $\delta$  (ppm): 177.70, 170.10, 135.70, 131.00, 126.30, 122.40, 120.30, 119.20, 111.30, 102.20, 63.40, 23.20, 23.10; IR (KBr)  $\nu$ : 3027 (arom. CH stretch), 2953 (aliph. CH stretch), 2900 (OH), 1715 (CO), 1610–1655 (C=N); Anal. Calcd for  $C_{15}H_{18}N_2O_2$  (258.32): C, 69.74%; H, 7.02%; O, 12.39%; N, 10.84%. Found: C, 69.38%; H, 6.76%; N, 10.46%.

#### 2-((1*H*-Indol-3-yl) methyleneamino)-6-aminohexanoic Acid (18)

Yield 86%; mp 114 °C;  $^1H$ -NMR (400 MHz, DMSO- $d_6$ )  $\delta$  (ppm): 11.00 (s, 1H, COOH), 9.50 (s, 1H, NH), 7.50 (s, 1H, CH=N), 7.11–7.55 (m, 5H, Ar-H), 2.60 (t, 2H, N-CH<sub>2</sub>), 2.30 (t, 1H, CH), 2.00 (s, 2H, NH<sub>2</sub>), 1.70 (m, 2H, CH-CH<sub>2</sub>), 1.51 (m, 4H, 2CH<sub>2</sub>);  $^{13}C$ -NMR (400 MHz, DMSO- $d_6$ )  $\delta$  (ppm): 177.70, 161.10, 135.70, 131.00, 126.30, 122.40, 120.30, 119.20, 111.30, 102.20, 66.20, 61.80, 42.30, 38.00, 32.70; IR (KBr)  $\nu$ : 3380 (NH<sub>2</sub>), 3027 (arom. CH stretch), 2953 (aliph. CH stretch), 2900 (OH), 1715 (CO), 1610–1655 (C=N); Anal. Calcd for  $C_{15}H_{19}N_3O_2$  (273.33): C, 65.91%; H, 7.01%; O, 11.71%; N, 15.37%. Found: C, 65.45%; H, 6.75%; N, 15.16%.

#### 2-((1*H*-Indol-3-yl)methyleneamino)-4-amino-4-oxobutanoic Acid (19)

Yield 93%; mp 181 °C;  $^1H$ -NMR (400 MHz, DMSO- $d_6$ )  $\delta$  (ppm): 11.00 (s, 1H, COOH), 9.50 (s, 1H, NH), 7.50 (s, 1H, CH=N), 7.11–7.55 (m, 5H, Ar-H), 6.00 (s, 2H, NH<sub>2</sub>), 2.65 (t, 1H, CH), 2.31–2.41 (d, 2H, CH<sub>2</sub>);  $^{13}C$ -NMR (400 MHz, DMSO- $d_6$ )  $\delta$  (ppm): 177.70, 174.80, 161.10, 135.70, 131.00, 126.30, 122.40, 120.30, 119.20, 111.30, 102.20, 63.00, 37.20; IR (KBr)  $\nu$ : 3390 (NH<sub>2</sub>), 3027 (arom. CH stretch), 2953 (aliph. CH stretch), 2900 (OH), 1715 (CO), 1610–1655 (C=N); Anal. Calcd for  $C_{13}H_{13}N_3O_3$  (259.26): C, 60.22%; H, 5.05%; O, 18.51%; N, 16.21%. Found: C, 59.88%; H, 4.82%; N, 15.96%.

#### 2-((1*H*-indol-3-yl)methyleneamino)-2-phenylacetic Acid (20)

Yield 94%; mp 166 °C;  $^1H$  NMR (400 MHz, DMSO- $d_6$ )  $\delta$  (ppm):  $^1H$  NMR (400 MHz, DMSO- $d_6$ )  $\delta$  (ppm): 11.00 (s, 1H, COOH), 9.50 (s, 1H, NH), 7.50 (s, 1H, CH=N), 7.31–7.72 (m, 5H, Ar-H), 7.00–7.29 (m, 5H, Ar-H), 3.75 (s, 1H, CH);  $^{13}C$  NMR (400 MHz, DMSO- $d_6$ )  $\delta$  (ppm): 178.20, 161.10, 138.70, 135.70, 131.00, 130.00, 129.40, 127.80, 126.30, 122.40, 120.30, 119.20, 111.30, 102.20, 65.20; IR (KBr)  $\nu$ : 3027 (arom. CH stretch), 2953 (aliph. CH stretch), 2900 (OH), 1715 (CO), 1610–1655 (C=N); Anal. Calcd for  $C_{17}H_{14}N_2O_2$  (278.31): C, 73.37%; H, 5.07%; O, 11.50%; N, 10.07%. Found: C, 72.95%; H, 4.87%; N, 9.46%.

## 2.2. In Silico Study

The three-dimensional coordinate files of the target enzymes hexokinase (1bdg) and NADH oxidoreductase (3m9s) were obtained from the Protein Data Bank (<http://www.rcsb.org/pdb/> accessed on 13 April 2021) [32]. The chemical structures of the new Schiff base compounds were sketched using ChemDraw Ultra 7.0 and then converted into SDF format using the Open Babel GUI tool [33]. Two in-house libraries of all the synthesized Schiff base molecules were generated for the docking process. The enzyme–ligand interaction study was performed using the PyRx virtual screening tool [34]. The Discovery Studio 3.5 tool was used to visualize the intermolecular interactions between the ligand molecules and enzymes. The prediction of molecular properties and drug-likeness of all synthesized compounds was achieved using the freely available tools Mol Inspiration, SwissADME, and admetSAR. Lipinski's rule of five (Ro5) was used to evaluate the drug-likeness of the prepared molecules [MW  $\leq$  500, HBA (2.0–20.0); HBD (0.0–6.0); logp < 5;

N rotatable  $\leq 10$ ; topological polar surface area (TPSA)  $\leq 140$ ; % (HIA<sup>+</sup>)  $> 80\%$  high,  $<25\%$  low; volume (500–2000)].

### 2.3. In Vitro Anticancer Studies on Predicted Compounds

The potent compounds in docking studies were selected to study their anticancer effect using MTT assay and then subjected to further analyses.

#### 2.3.1. Cell Culture, Maintenance, and Treatment

The estrogen receptor-positive breast cancer cell line MCF-7, triple-negative breast cancer cell line MDA-231, and pancreatic cancer cell line (PCL), along with the human normal epithelial amnion cell line WISH as a model for normal cells, were maintained and cultured in Dulbecco's Modified Eagle's Medium with 10% fetal bovine serum (all obtained from Gibco-BRL, New York, NY, USA) and 1% penicillin/streptomycin under a 5% CO<sub>2</sub> and 95% humidified atmosphere at 37 °C in a CO<sub>2</sub> incubator. All cells were provided by the National Cancer Institute (Cairo University, Giza Egypt). The cells were incubated for 48 h with selected compounds at different concentrations (0–200 g/mL) and tamoxifen (TAM) as a reference drug (0–100 g/mL) and then subjected to analysis.

#### 2.3.2. Cell Cytotoxicity Assay by MTT

In vitro cell viability was tested using the tetrazolium 3-(4,5-dimethylthiazol-2-yl)-2,5-diphenyl-tetrazolium bromide (MTT) assay. The cells were separately seeded in a 96-well plate ( $1 \times 10^4$  cells/well, 100  $\mu$ L/well) containing appropriate medium and incubated with the drug at different doses for 48 h. Then, the cells were incubated with 5 mg/mL MTT (Gibco-BRL, New York, NY, USA) for 4 h, followed by replacement of the medium with 100  $\mu$ L of DMSO (Sigma-Aldrich, St. Louis, MO, USA) and vortexing for 20 min. Absorbance was recorded at 570 nm using a Model 680 microplate reader (Bio-Rad, Hercules, CA, USA) [35]. The concentration of the selected compound and TAM inhibiting 50% of cells (IC<sub>50</sub>) was calculated using the sigmoidal curve with GraphPad (Prism) statistical software.

#### 2.3.3. Cell Cycle Analysis

Cell cycle phase analysis was performed by flow cytometry following the method of Darzynkiewicz et al. [36] with some modifications. Briefly, following trypsinization, MCF-7 and MDA-231 cells were centrifuged at 4500 rpm for 5 min, washed twice, resuspended in warm PBS, fixed with ice-cold absolute ethanol, and then incubated at  $-20$  °C for 24 h. After two washes with PBS, the cells were resuspended in propidium iodide (PI) solution containing 100  $\mu$ L (0.05 mg/mL) of PI, 50  $\mu$ L (0.2 mg/mL) of RNase A, and 0.1% *v/v* Triton X-100 in PBS and incubated in the dark for 30–60 min at room temperature. Finally, the pellet was washed with 1X PBS and resuspended in 300  $\mu$ L 1X PBS and analyzed using an Accuri C6 flow cytometer (Becton Dickinson, Franklin Lake, BD, USA) with PE  $\times$  FL2 channels.

#### 2.3.4. QPCR Analysis

The qPCR was carried out on treated and control cells to assess Bax, p53, and Bcl-2 mRNA expression. Briefly, total RNA was extracted using RNeasy Plus Minikit (Qiagen, Hilden, Germany) following the manufacturer's protocol and as previously described by Kvastad et al. [37]. The quality of RNA was assessed by 1% agarose gel electrophoresis and the concentration was determined using Nanodrop (Q5000, Quawell, 1920 city, Chester, PA, USA). For cDNA synthesis, total RNA was reverse-transcribed with RevertAid H Minus Reverse Transcriptase following the manufacturer's instructions (Thermo Fisher Scientific, Waltham, MA, USA). Real-time PCR was performed using Power SYBR Master Mix (Thermo Fisher Scientific) on an Applied Biosystems 7500 system (Applied Biosystems, Waltham, MA, USA), following the standard program of the reaction cycle of 95 °C for 10 min, followed by 40–45 cycles at 95 °C for 15 s and at 60 °C for 1 min, as recommended by

the manufacturer. Samples of cDNA were run in triplicate. All data were then normalized to the endogenous control, GAPDH, a housekeeping gene. The quantity critical thresholds (Ct) of the target gene were normalized with the quantity (Ct) of GAPDH. Fold change in gene expression was calculated using the comparative threshold cycle ( $2^{-\Delta\Delta CT}$ ) method of Livak and Schmittgen [38]. For the treated groups,  $2^{-\Delta\Delta CT}$  assessment was used to determine the fold change in gene expression relative to the control untreated group. The primer sequences used in this study are provided in Table 1.

**Table 1.** Primer sequences used in qRT-PCR.

Gene	Forward Primer (5—/3)	Reverse Primer (5—/3)
Bax	GGCTGGACACTGGACTTCCT	GGTGAGGACTCCAGCCACAA
P53	TAACAGTTCCTGCATGGGCGGC	AGGACAGGCACAAACACGCACC
Bcl-2	TTCGACAGAGATGTCCAGTCA	TTCAGAGACAGCCAGGAGAA
GAPDH	TGTGTCCGTCGTGGATCTGA	CCTGCTTACCACCTTCTTGA

### 2.3.5. Detection of Hexokinase Activity Level (ELISA)

Six-well tissue culture plates were seeded with  $1 \times 10^5$  MCF-7 and MDA-231 cells and left for 24 h under optimal culture conditions to obtain a confluent sheet of cells, which were then treated for 48 h. Subsequently, the cells were harvested, and their lysate was extracted to estimate the levels of hexokinase activity using human ELISA kits following the manufacturer's instructions (cat. No. MAK091; Sigma-Aldrich).

### 2.3.6. Estimation of Oxidative/Antioxidant Biomarkers

Six-well tissue culture plates were seeded with  $1 \times 10^5$  MCF-7 and MDA-231 cells and left for 24 h under optimal culture conditions to obtain a confluent layer of cells, which were then treated for 48 h. Subsequently, the cells were washed with PBS and scraped. The scraped cells were incubated in lysis buffer [20 mM Tris-HCl (pH 7.5), 150 mM NaCl, 1 mM Na<sub>2</sub>EDTA, 1% Triton, and 2.5 mM sodium pyrophosphate]. Then, the cells were centrifuged at 15,000 rpm and 4 °C for 15 min. The supernatant was used to measure the levels of malondialdehyde (MDA) and reduced glutathione (GSH) [39] and the protein concentration was measured using the Bradford assay [40].

### 2.3.7. Immunoblotting Analysis

Immunoblotting was performed following the method reported by Mruk and Cheng [41]. In this method, the proteins are extracted from cells using ice-cold lysis buffer 50 mM Tris-HCl pH 7.4, 150 mM NaCl, 1% Nonidet P-40, 1 mM ethylenediaminetetraacetic acid (EDTA), 1X Protease Inhibitor Cocktail]. The protein was quantified using a Bradford assay kit (Thermo Scientific), and equal quantities of protein (20 µg) were resolved by 12% SDS-polyacrylamide gel electrophoresis and then transferred onto a polyvinylidene difluoride (PVDF) membrane. This membrane was blocked with 5% skimmed milk for 1 h at room temperature and then incubated with specific primary antibodies phospho-AMPK (2535) (1:1000) and phospho-mTOR (29771) (1:1000). Blots were incubated with horseradish peroxidase (HRP)-conjugated goat anti-rabbit IgG (H + L) (ab205718) (1:1000) and visualized using enhanced chemiluminescence (Pierce ECL Western blotting substrate) and Alliance gel doc (Alliance 4.7 Gel doc, Alliance, UK). UV Tec software (UK) was used to semi-quantify the protein bands. The density of each band was normalized using β-actin (SC-69879).

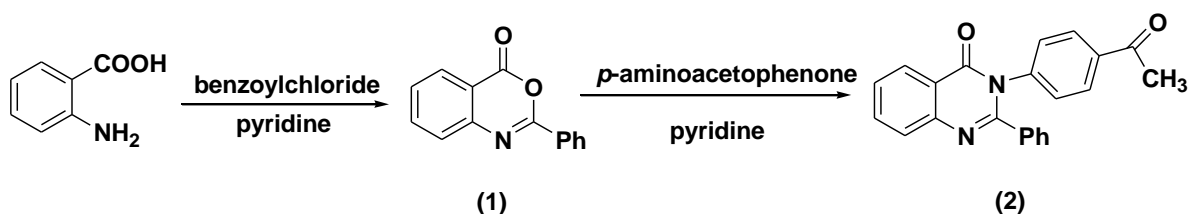
### 2.3.8. Statistical Analysis

The experimental data are expressed as mean ± SE. The significance of differences among the various treated groups and control was analyzed using one-way ANOVA followed by Tukey's test with GraphPad Prism 6 software (San Diego, CA, USA). Differences were considered to be significant at  $p < 0.05$ .

### 3. Results and Discussion

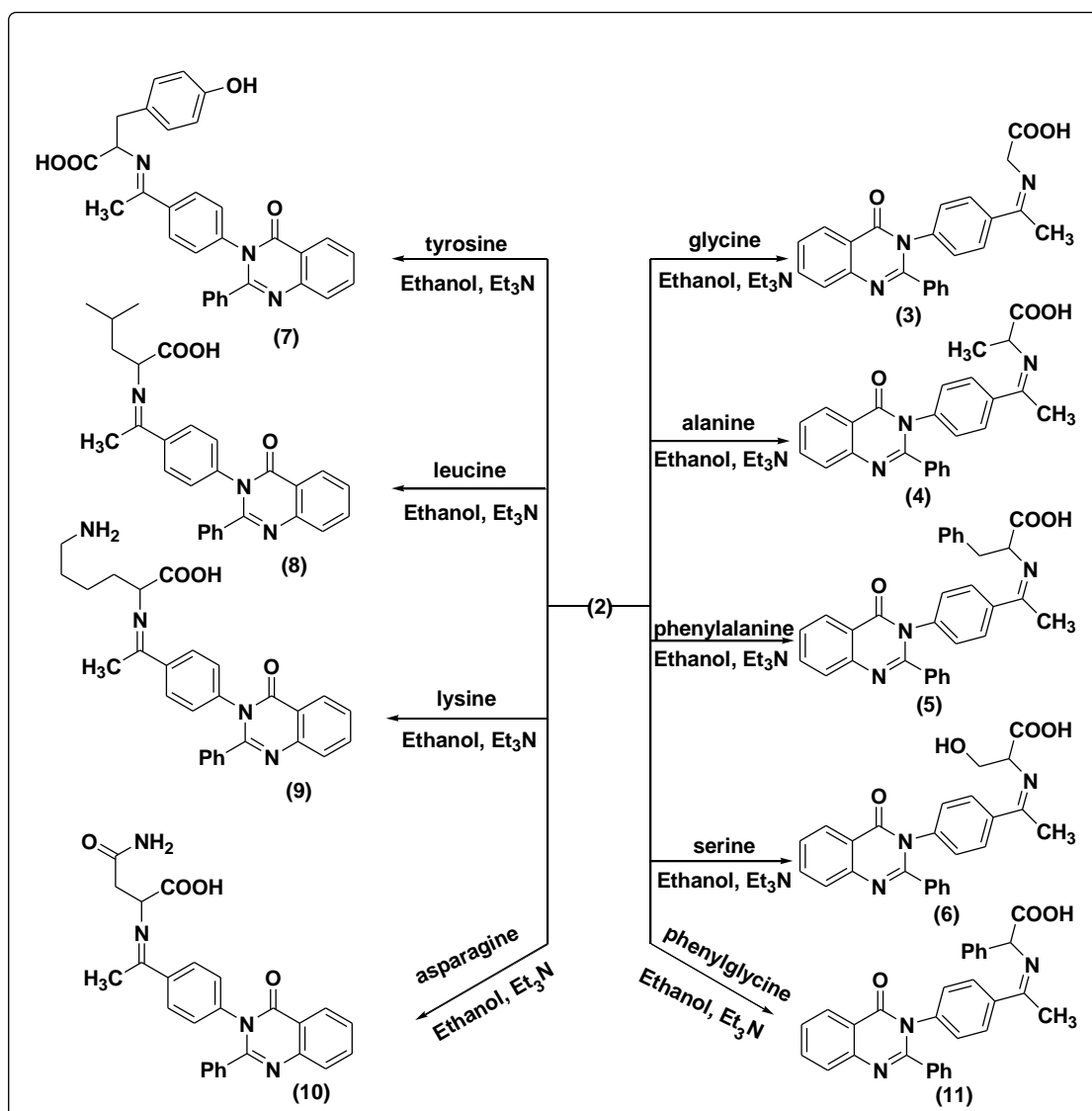
#### 3.1. Chemistry of the Synthesized Compounds

2-Phenyl-4*H*-benzo[*d*][1,3]oxazin-4-one **1** was synthesized and characterized as previously described in the literature [29]. In the present study, the synthesis of 3-(4-acetylphenyl)-2-phenylquinazolin-4(3*H*)-one **2** was successfully achieved by refluxing compound **1** with *p*-aminoacetophenone in the presence of anhydrous pyridine, to give a high yield of 82%, as shown in Scheme 1.



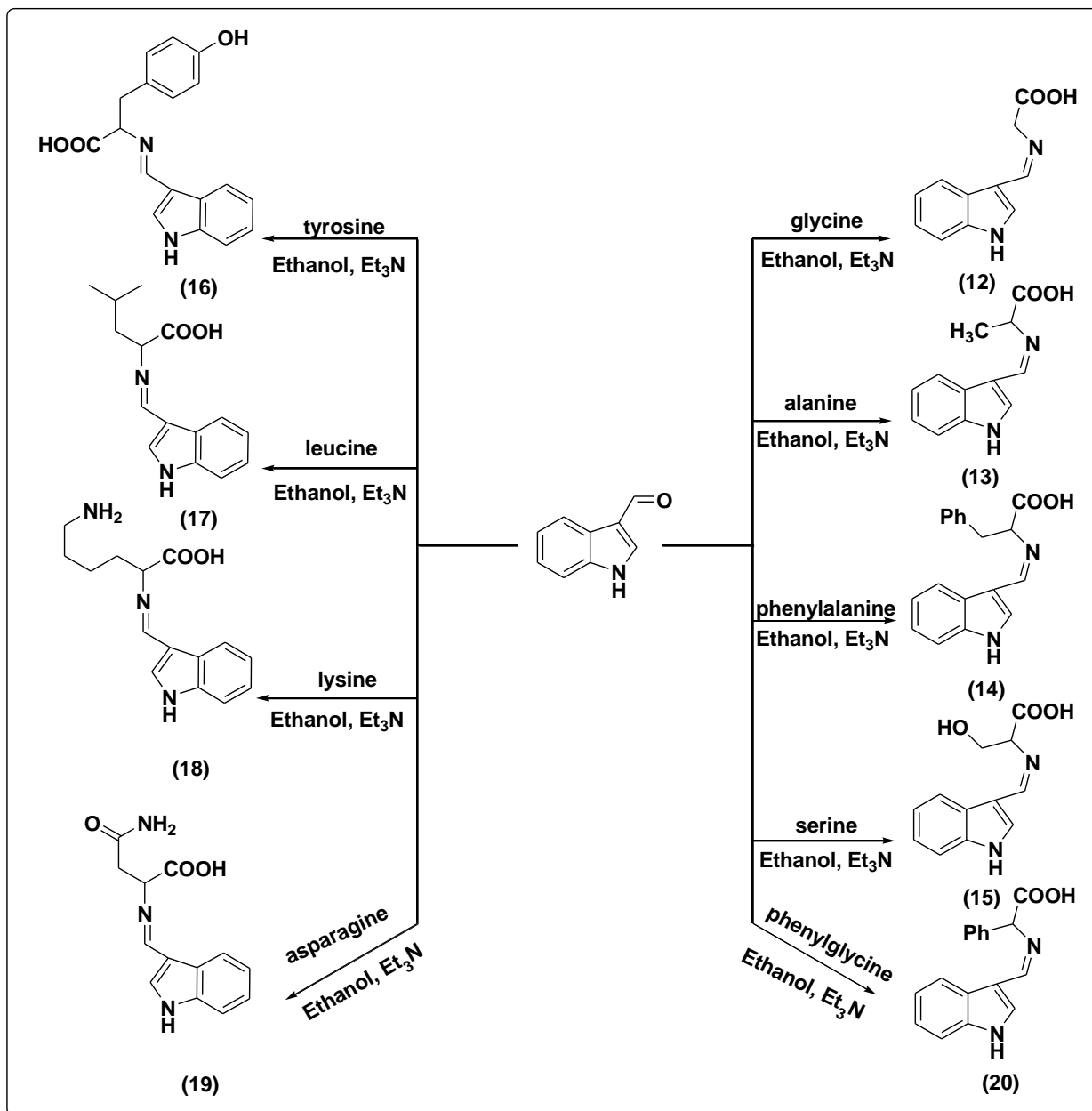
Scheme 1. The synthesis pathway of compounds **1** and **2**.

The suggested Schiff base compounds **3–11** were synthesized by a condensation reaction of compound **2** with various amino acids in the presence of triethylamine (TEA) and ethanol as solvent, as shown in Scheme 2.



Scheme 2. The synthesis pathway of compounds **3–11**.

Furthermore, Schiff bases **12–20** were synthesized by the condensation reaction of indol-3-carboxaldehyde with different amino acids in the presence of  $\text{Et}_3\text{N}$  and ethanol as solvent, as shown in Scheme 3.



**Scheme 3.** The synthesis pathway of compounds **12–20**.

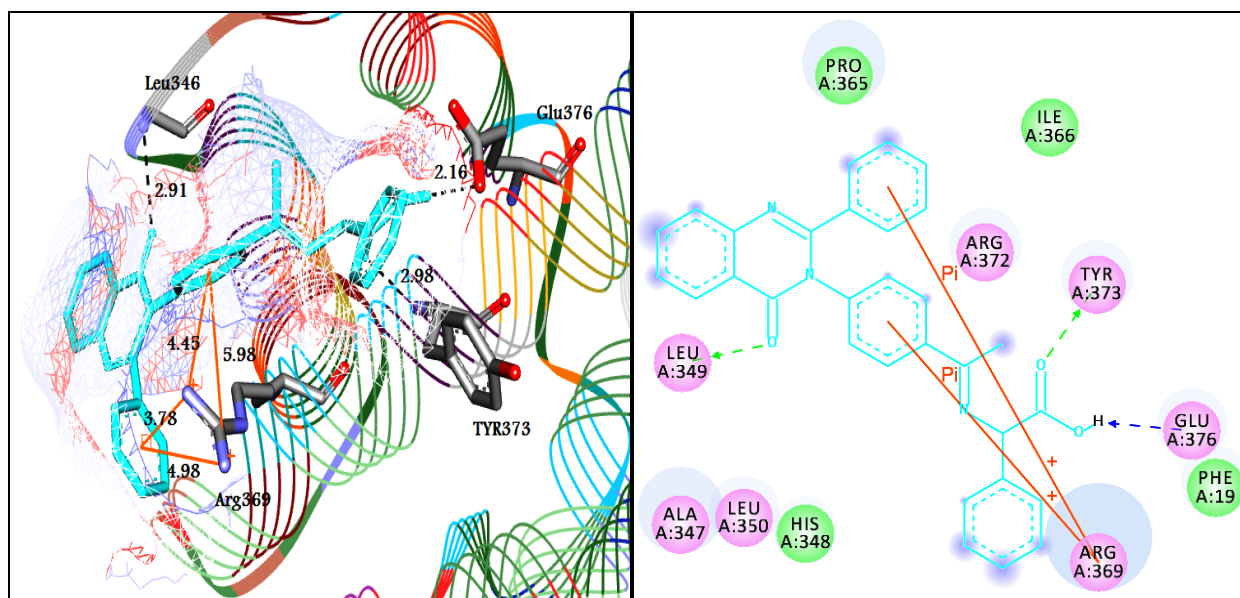
All synthesized compounds **3–20** were characterized by spectroscopic techniques, such as FT-IR and NMR spectroscopy, and elemental analysis as shown in the Supplementary Materials. The FT-IR spectra of Schiff bases showed that the band of  $-\text{C}=\text{N}$  imine stretching vibration appeared for the Schiff bases in the range of  $1610\text{--}1655\text{ cm}^{-1}$ .

### 3.2. In Silico Docking Study

In this study, the binding mode of quinazolinone **3–11** and indole **12–20** Schiff base derivatives with the prospective crystal structures of hexokinase HK (PDB ID: 1bdg) and NADH oxidoreductase (PDB ID: 3m9s) enzymes was investigated. In silico molecular docking studies [42] were performed for all compounds using molecular docking in the PyRx tool, to explore and explain the orientation of molecules bound in the active sites of

the target enzymes. The eighteen molecules showed good binding energy, indicating that they were successfully docked to the active site of the target enzymes HK and NADH [43]. Figures 1 and 2 represent the molecular interactions between the best docked compounds (11 and 20), with the target enzymes. Different interactions, as well as the binding energies, are presented in Table 2. The 2D interactions of the other compounds are included in the Supplementary Materials as Figures S37 and S38.

### Compound 11-HK complex



### Compound 11-NADH oxidoreductase

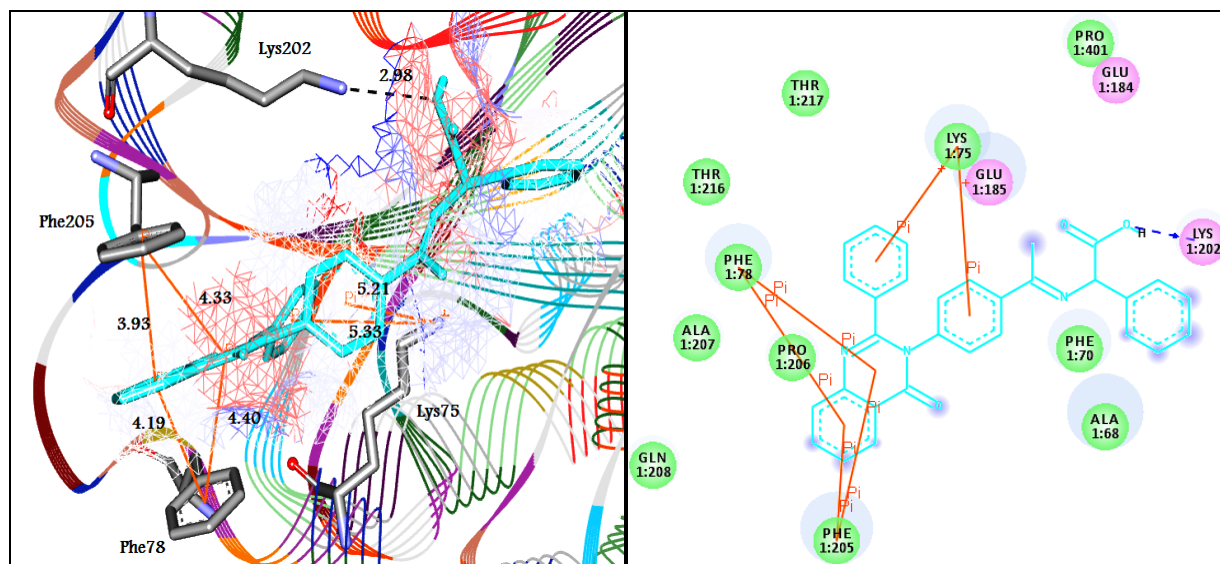


**Figure 1.** Depicted the interaction between quinazolin-4(3H)-one analog 11 with hexokinase and NADH oxidoreductase enzymes. Left side representing 3D and the right side representing 2D complex enzyme-ligand interaction. In 3D representation, the docked compounds are represented in cyan stick models, while the binding active residues are represented in grey stick models. The HB interactions are shown in the black dotted line while the  $\pi$ -stacking interactions are shown in the orange line. In 2D, the docked compounds are represented in cyan stick color, while the binding active residues are represented in 3 letter codes. The HB interactions are shown in green and blue dotted lines while the  $\pi$ -stacking interactions are shown in the orange line.

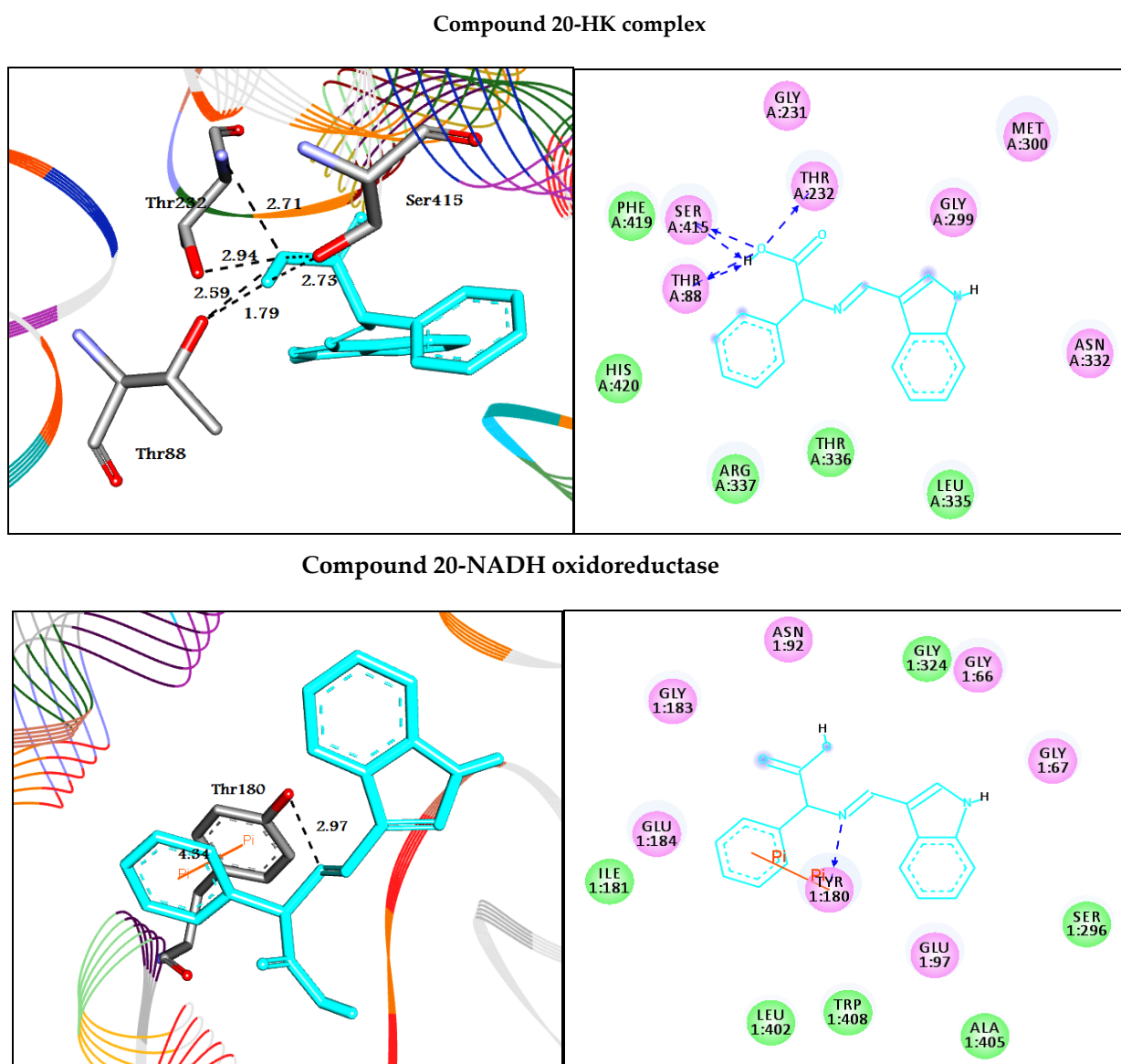


**Figure 2.** Depicted the interaction between indole derivative 20 with hexokinase HK and NADH oxidoreductase enzymes. Left side representing 3D and the right side representing 2D complex enzyme-ligand interaction. In the 3D representation, the docked compounds are represented in cyan stick models, while the binding active residues are represented in grey stick models. The HB interactions are shown in the black dotted line while the  $\pi$ -stacking interactions are shown in the orange line. In 2D, the docked compounds are represented in cyan stick color, while the binding active residues are represented in 3 letter codes. The HB interactions are shown in green and blue dotted lines while the  $\pi$ -stacking interactions are shown in the orange line.

**Table 2.** Depicted the binding energies ( $\Delta G_{\text{bind}}$ ) and molecular interactions between the docked compounds 3–20 with the prospective enzymes Hexokinase and NADH oxidoreductase.

HK			NADH		
$(\Delta G_{\text{bind}})$	Docked Complex (Amino Acid–Ligand) Interactions	Distance (Å)	$(\Delta G_{\text{bind}})$	Docked Complex (Amino Acid–Ligand) Interactions	Distance (Å)
3	<b>H-bonds</b> Glu220:OE1—compound 3 <b><math>\pi</math>-<math>\sigma</math> interactions</b> Pro105:CD—compound 3	2.38  3.61	-9.4	<b>H-bonds</b> Lys202:NZ—compound 3	2.98
				<b><math>\pi</math>-<math>\pi</math> interactions</b> Phe205—compound 3	4.28
				Phe205—compound 3	4.29
				Phe78—compound 3	3.93
				Phe78—compound 3	4.23
				<b><math>\pi</math>-cation interactions</b> Lys75:NZ—compound 3 Lys75:NZ—compound 3	5.42 5.25
4	<b>H-bonds</b> Ile114:N—compound 4 <b><math>\pi</math>-<math>\sigma</math> interactions</b> Met300:CA—compound 4	3  3.87	-9.5	<b>H-bonds</b> Lys202:NZ—compound 4	3
				<b><math>\pi</math>-<math>\pi</math> interactions</b> Phe205—compound 4	4.17
				Phe205—compound 4	4.18
				Phe78—compound 4	4.07
				Phe78—compound 4	4.32
				<b><math>\pi</math>-cation interactions</b> Lys75:NZ—compound 4 Lys75:NZ—compound 4	5.71 5.36
5	<b><math>\pi</math>-<math>\sigma</math> interactions</b> Met300:CA—compound 5	3.88	-10.7	<b>H-bonds</b> Glu184:OE2—compound 5	2.11
				<b><math>\pi</math>-<math>\pi</math> interactions</b> Phe205—compound 5	4.28
				Phe205—compound 5	3.95
				Phe78—compound 5	4.37
				Phe78—compound 5	4.21
				<b><math>\pi</math>-cation interactions</b> Lys75:NZ—compound 5 Lys75:NZ—compound 5 Lys75:NZ—compound 5	5.38 5.43 5.91
6	<b>H-bonds</b> Tyr90:N—compound 6 <b><math>\pi</math>-<math>\sigma</math> interactions</b> Met300:CA—compound 6	2.95  3.91	-9.3	<b>H-bonds</b> Lys202:NZ—compound 6 Glu185:OE2—compound 6	2.99 2.46
				<b><math>\pi</math>-<math>\pi</math> interactions</b> Phe205—compound 6	4.12
				Phe205—compound 6	4.24
				Phe78—compound 6	4.08
				Phe78—compound 6	4.28
				<b><math>\pi</math>-cation interactions</b> Lys75:NZ—compound 6 Lys75:NZ—compound 6	5.55 5.4
7	<b>H-bonds</b> Thr88:OG1—compound 7 Ile114:N—compound 7 Ile114:O—compound 7 Thr232:OG1—compound 7	2.95 2.96 2.94 2.65	-11.0	<b>H-bonds</b> Asn92:ND2—compound 7 Lys202:NZ—compound 7	2.95 2.87
				<b><math>\pi</math>-<math>\pi</math> interactions</b> Phe205—compound 7	4.1
				Phe205—compound 7	4.18
				Phe78—compound 7	4.46
				Phe78—compound 7	3.99
				<b><math>\pi</math>-cation interactions</b> Lys75:NZ—compound 7	5.88

Table 2. Cont.

		HK		NADH		
	( $\Delta G_{\text{bind}}$ )	Docked Complex (Amino Acid–Ligand) Interactions	Distance (Å)	( $\Delta G_{\text{bind}}$ )	Docked Complex (Amino Acid–Ligand) Interactions	Distance (Å)
8	−7.7	$\pi$ - $\sigma$ interactions Pro105:CD—compound 8		−12.8	<b>H-bonds</b>	2.93
					Glu97:OE1—compound 8	2.89
					Tyr180:OH—compound 8	
					<b><math>\pi</math>-<math>\pi</math> interactions</b>	
					Phe205—compound 8	4.14
					Phe205—compound 8	4.24
					Phe78—compound 8	4.35
9	−7.2	<b>H-bonds</b> Lys62:NZ—compound 9 Glu266:OE1—compound 9 Lys267:NZ—compound 9 <b><math>\pi</math>-cation interactions</b> Lys62:NZ—compound 9		−9.5	<b>H-bonds</b>	2.92
					Lys75:NZ—compound 9	2.35
					Gly183:O—compound 9	
					<b><math>\pi</math>-<math>\pi</math> interactions</b>	
					Phe205—compound 9	4.43
					Phe205—compound 9	4.29
					Phe78—compound 9	4.31
10	−8.6	$\pi$ - $\sigma$ interactions Met300:CA—compound 10	3.83	−9.6	<b>H-bonds</b>	2.23
					Glu184:OE2—compound 10	2.88
					Lys202:NZ—compound 10	
					<b><math>\pi</math>-<math>\pi</math> interactions</b>	
					Phe205—compound 10	4.37
					Phe205—compound 10	3.94
					Phe78—compound 10	4.41
11	−8.8	<b><math>\pi</math>-cation interactions</b> Arg369:NH1—compound 11 Arg369:NH1—compound 11 Arg369:NH2—compound 11 Arg369:NH2—compound 11		−13.0	<b>H-bonds</b>	2.91
					Leu349:N—compound 11	2.98
					Tyr373:N—compound 11	2.16
					Glu376—compound 11	
					Lys75:NZ—compound 10	5.38
					Lys75:NZ—compound 10	5.3
					12	
Lys202:NZ—compound 11	2.98					
<b><math>\pi</math>-<math>\pi</math> interactions</b>						
Phe205—compound 11	4.33					
Phe205—compound 11	3.93					
Phe78—compound 11	4.4					
Phe78—compound 11	4.19					
13		<b>H-bonds</b> Gly303:N—compound 13 Thr336:OG1—compound 13		−8.0	<b>H-bonds</b>	2.96
					Asn92:ND2—compound 12	2.96
					Asn92:ND2—compound 12	3.01
					Tyr180:O—compound 12	1.86
					<b><math>\pi</math>-<math>\pi</math> interactions</b>	
					Tyr180—compound 12	4.72
					Tyr180—compound 12	3.98
13		<b>H-bonds</b> Gly303:N—compound 13 Thr336:OG1—compound 13		−8.0	<b>H-bonds</b>	2.95
					Asn92:ND2—compound 13	2.98
					Tyr180:O—compound 13	1.81
					<b><math>\pi</math>-<math>\pi</math> interactions</b>	
Tyr180—compound 13	4.74					
Tyr180—compound 13	4.04					

Table 2. Cont.

HK			NADH			
( $\Delta G_{\text{bind}}$ )	Docked Complex (Amino Acid–Ligand) Interactions	Distance (Å)	( $\Delta G_{\text{bind}}$ )	Docked Complex (Amino Acid–Ligand) Interactions	Distance (Å)	
14	<b>H-bonds</b>		−8.4	<b>H-bonds</b>		
	Thr88:N—compound 14	2.95		Tyr180:O—compound 14	2.94	
	Thr88:OG1—compound 14	2.92		<b><math>\pi</math>-<math>\pi</math> interactions</b>		
	Thr232:N—compound 14	2.85		Tyr180—compound 14	4.75	
	Thr232:N—compound 14	2.85				
	Thr232:OG1—compound 14	2.99				
	Gly233:N—compound 14	2.94				
	<b><math>\pi</math>-cation interactions</b>					
Lys418:NZ—compound 14	4.02					
Lys418:NZ—compound 14	4.43					
15	<b>H-bonds</b>		−7.8	<b>H-bonds</b>		
	Thr88:N—compound 15	2.9		Asn92:ND2—compound 15	2.93	
	Thr88:OG1—compound 15	2.87		Ser96:N—compound 15	2.93	
	Thr232:N—compound 15	2.98		Ser96:N—compound 15	2.89	
	Thr232:N—compound 15	2.92		<b><math>\pi</math>-<math>\pi</math> interactions</b>		
	Thr232:OG1—compound 15	2.99		Tyr180—compound 15	4.96	
	Gly233:N—compound 15	2.89		Tyr180—compound 15	4.16	
	Asp209:OD2—compound 15	2.08				
16	<b>H-bonds</b>		−8.6	<b>H-bonds</b>		
	Thr88:N—compound 16	3.02		Asn92:ND2—compound 16	2.81	
	Thr88:OG1—compound 16	2.33		Ser100:OG—compound 16	2.64	
	Thr232:N—compound 16	2.86		Lys102:NZ—compound 16	2.95	
	Thr232:OG1—compound 16	2.77		<b><math>\pi</math>-<math>\pi</math> interactions</b>		
	Thr232:OG1—compound 16	2.31		Tyr180—compound 16	5.15	
	Ser415:OG—compound 16	2.89		Tyr180—compound 16	4.28	
17	<b>H-bonds</b>		−8.1	<b>H-bonds</b>		
	Thr88:N—compound 17	2.96		Gly66:O—compound 17	2.4	
	Thr88:OG1—compound 17	2.82		Asn92:ND2—compound 17	2.97	
	Thr88:OG1—compound 17	2.23		<b><math>\pi</math>-<math>\pi</math> interactions</b>		
	Thr232:N—compound 17	2.99		Tyr180—compound 17	4.9	
	Thr232:N—compound 17	2.98		Tyr180—compound 17	4.13	
	Thr232:OG1—compound 17	3				
	<b><math>\pi</math>-cation interactions</b>					
Lys418:NZ—compound 17	3.58					
Lys418:NZ—compound 17	4.4					
18	<b>H-bonds</b>		−8.0	<b>H-bonds</b>		
	Thr88:N—compound 18	3		Asn92:ND2—compound 18	3.09	
	Thr88:OG1—compound 18	2.89		Asn92:ND2—compound 18	2.89	
	Thr88:OG1—compound 18	2.19		Asp103:OD2—compound 18	1.93	
	Thr232:N—compound 18	2.99		<b><math>\pi</math>-<math>\pi</math> interactions</b>		
	Thr232:N—compound 18	2.98		Tyr180—compound 18	5.03	
	Thr232:OG1—compound 18	2.95		Tyr180—compound 18	4.55	
	Asp413:OD2—compound 18	2.37				
<b><math>\pi</math>-cation interactions</b>						
Lys418:NZ—compound 18	3.63					
Lys418:NZ—compound 18	4.52					
19	<b>H-bonds</b>		−8.4	<b>H-bonds</b>		
	Thr88:OG1—compound 19	2.42		Asn92:ND2—compound 19	2.97	
	Asn89:ND2—compound 19	2.99		Ser96:N—compound 19	2.95	
	Asp413:OD1—compound 19	2.4		Glu97:N—compound 19	3.06	
	Asp413:OD2—compound 19	2.4		<b><math>\pi</math>-<math>\pi</math> interactions</b>		
	Glu446:O—compound 19	2.39		Tyr180—compound 19	4.85	
	<b><math>\pi</math>-sigma interactions</b>			Tyr180—compound 19	4.14	
Gly414:CA—compound 19	3.86					

Table 2. Cont.

HK			NADH				
( $\Delta G_{\text{bind}}$ )	Docked Complex (Amino Acid–Ligand) Interactions	Distance (Å)	( $\Delta G_{\text{bind}}$ )	Docked Complex (Amino Acid–Ligand) Interactions	Distance (Å)		
20	<b>H-bonds</b>		−10.0	<b>H-bonds</b>			
	Thr88:OG1—compound 20	2.59		Tyr180:OH—compound 20	2.97		
	Thr88:OG1—compound 20	1.79					
	Thr232:N—compound 20	2.94				<b><math>\pi</math>-<math>\pi</math> interactions</b>	
	Thr232:OG1—compound 20	2.71				Tyr180—compound 20	4.34
	Ser415:OG—compound 20	2.73					
Ser415:OG—compound 20	2.31						

### Docking study against hexokinase enzyme

For the Schiff base compounds containing quinazolinone moiety 3–11 (first library), the placement of compound 3 into a hexokinase active site exhibited HB and  $\pi$ - $\sigma$  interactions with Glu220 and Pro105 at distances of 2.38 and 3.61 Å, respectively. Compounds 4–6 and 10 were stabilized in the pocket of the target enzyme through  $\pi$ - $\sigma$  interactions with Met300 at 3.87, 3.88, 3.91, and 3.83 Å, respectively. In addition, compounds 4 and 6 formed HB with Ile114, and Tyr90 at 3.00 and 2.95 Å, respectively. Moreover, compound 11 with the highest binding energy of the first library (−8.8 kcal/mol) docked to the hexokinase enzyme through hydrogen bonds and  $\pi$ -cation interactions. It formed molecular interactions with the amino acid residues Leu349, Tyr373, Glu376, and Arg369 at distances of 2.91, 2.98, 2.16, 4.45, 3.78, 5.98, and 4.98 Å, respectively.

On the other hand, regarding the Schiff base compounds containing indole moiety 12–20 (second library), all compounds except 13 and 19 formed HB interactions with residue Thr232. Compound 12 docked to the target through HB with residues Thr232 and Gly233 at 3.10, 2.93, and 2.83 Å, respectively. Compound 13 formed two HB with Gly303 and Thr336. Additionally, compounds 14–18 and 20 were completely enfolded in the active site forming similar interactions through the amino acid residues Thr88, Thr232, Gly233, Asp209, Asp413, Ser415, and Glu446. Furthermore, compounds 12, 14, 17, and 18 exhibited  $\pi$ -cation interactions with the residue Lys418. Finally, molecule 20 with the highest binding energy of the second library (−7.9 kcal/mol) was successfully docked to the target enzyme hexokinase through HB interactions.

### Docking study against NADH oxidoreductase enzyme

For the first library, all of compounds 3–11 docked to the target enzyme NADH oxidoreductase through four  $\pi$ - $\pi$  interactions with residues Phe78 and Phe205. They also formed  $\pi$ -cation interactions with the residue Lys75, with the exceptions of 8 and 9. In addition, they exhibited similar HB to Lys202. Compound 11 with the highest affinity to NADH oxidoreductase enzyme (−13.0 kcal/mol) formed one H-bond, four  $\pi$ - $\pi$ , and two  $\pi$ -cation interactions with residues Lys202, Phe205, Phe78, and Lys75 at distances of 2.98, 4.33, 3.93, 4.40, 4.19, 5.21, and 5.33 Å, respectively.

On the other hand, all of the compounds related to the Schiff bases containing indole moiety (the second library) 12–20 formed  $\pi$ - $\pi$  interactions with Tyr180. In addition, they formed HB interactions with the target enzyme, though various residues, such as Asn92, Ser96, Ser100, Asp103, and Tyr180. Molecule 20 docked with NADH oxidoreductase enzyme with high affinity (−10.0 kcal/mol) through different types of non-covalent interaction, such as HB and  $\pi$ - $\pi$  interactions with residue Tyr180 at 2.97 and 4.34 Å, respectively.

### ADMET properties and SAR analysis

The ADMET data of two quinazolinone and indole Schiff base compounds were predicted as shown in Table 3. The results clearly pointed out that all compounds, except 12–14 and 17 cannot pass the blood–brain barrier (BBB), which confirmed their good CNS safety profile. Further, it was found that the compounds can be absorbed by the intestine. Their molecular weights were in the acceptable range ( $\leq 500$  g/mol), with the exception

of compound 7. The results of in silico absorption percentage calculations showed high absorption percentage values (73–99%). Hence, it can be concluded that the compounds possess good absorption and distribution properties.

**Table 3.** ADMET and drug-likeness properties of all docked molecules 3–20.

Reference Range	Molecular Weight (g/mol)	BBB Permeant	% (HIA+)	logp	TPSA A <sup>2</sup>	HBA	HBD	N Rotatable	N Violations	Volume A [3]	GI Absorption	Bioavailability Score
	130–500		<25 Poor >80 High	<5	≤140	2–20	0–6	≤10	<5	500–2000		
3	397.43	No	90	3.06	84.56	6	1	5	0	354.67	High	0.56
4	411.45	No	98	2.84	84.56	6	1	5	0	371.26	High	0.56
5	487.55	No	97	4.30	84.56	6	1	7	0	442.91	High	0.56
6	427.25	No	95	1.87	104.79	7	2	6	0	379.52	High	0.56
7	503.55	No	88	3.83	104.79	7	2	7	1	450.39	High	0.56
8	453.53	No	91	4.15	84.56	6	1	7	0	421.45	High	0.56
9	468.55	No	88	2.35	110.58	7	3	9	0	433.19	High	0.55
10	454.48	No	91	2.73	127.65	8	3	7	0	401.77	High	0.56
11	473.53	No	96	4.44	84.56	6	1	6	0	426.11	High	0.56
12	202.21	Yes	73	0.26	65.45	4	2	3	0	180.08	High	0.85
13	216.24	Yes	87	0.04	65.45	4	2	3	0	196.67	High	0.85
14	292.34	Yes	81	1.50	65.45	4	2	5	0	268.32	High	0.85
15	232.24	No	80	- 0.93	85.68	5	3	4	0	204.93	High	0.56
16	308.33	No	83	1.02	85.68	5	3	5	0	276.34	High	0.56
17	258.32	Yes	75	1.35	65.45	4	2	5	0	246.86	High	0.85
18	273.43	No	85	- 0.45	91.48	5	4	7	0	258.61	High	0.55
19	259.26	No	90	- 0.07	108.55	6	4	5	0	227.18	High	0.56
20	278.31	No	99	2.75	65.45	4	2	4	0	251.52	High	0.85

Abbreviations and acceptable ranges are as follows; HBA, number of hydrogen bond acceptors (2.0–20.0); HBD, number of hydrogen bond donors (0.0–6.0); logp, logarithm of partition coefficient between n-octanol and water (<5); N rotatable, number of rotatable bonds (≤10); TPSA, topological polar surface area (≤140); Mol wt.: (130–500); % (HIA<sup>+</sup>) Human oral absorption: >80% high, <25% low; Volume: (500–2000).

The obtained TPSA values for molecules 3–20 were below 140 A<sup>2</sup>, indicating that the compounds had considerable permeability into the plasma membrane. All target compounds were in an acceptable range for HBD (1–4), HBA (4–8), and rotatable bonds (3–9). In addition, the compounds had high gastrointestinal (GI) absorption, confirming that they have excellent potential for absorption from the intestine after oral administration. All of the ligands had good bioavailability with scores ranging from 0.55 to 0.85, which is an indication that all compounds reached the circulatory system easily. Moreover, these compounds exhibited negative results on toxicity and carcinogenicity tests. The number of violations of Lipinski's rule of five is listed in Table 3, which showed that all molecules fulfilled this rule with zero violations, with the exception of compound 7, which represents the only Lipinski violation among these target compounds. Therefore, all molecules might be realistic drug candidates.

The structure-activity relationship (SAR) revealed why the combinations of Schiff base compounds (imines) with heterocyclic systems, such as quinazolinone and indole nucleus, azomethine linkage, and phenyl ring have attracted particular attention due to their potential applications in medicinal and pharmaceutical chemistry.

### 3.3. In Vitro Studies

From the in-silico studies, compounds 11 and 20 were selected to study their ability to be used as novel anticancer agents via the inhibition of mitochondrial complex I-associated hexokinase.

### 3.3.1. Cytotoxic Effect of Compounds 11, 20, and Tamoxifen (TAM)

In research on new anticancer agents, the most common screening methods are testing against a panel of different cancer cell lines. In this study, an MTT assay was carried out to determine the cytotoxic effect of compounds **11** and **20** on the proliferation of MCF-7, MDA-231, PCL, and the toxicity limit on the normal cell line WISH after 48 h (Figure 3). Compounds **11** and **20** exhibited significant cytotoxic effects on MCF-7, MDA-231, and PCL cancer cell lines as the  $IC_{50}$  values of compound **11** were  $64.05 \pm 0.14 \mu\text{g/mL}$  (0.135 mM),  $77.35 \pm 0.09 \mu\text{g/mL}$  (0.163 mM), and  $73.97 \pm 0.15 \mu\text{g/mL}$  (0.156 mM), respectively. The  $IC_{50}$  values of compound **20** against MCF-7, MDA-231, and PCL cell lines were  $54.41 \pm 0.08 \mu\text{g/mL}$  (0.195 mM),  $46.29 \pm 0.09 \mu\text{g/mL}$  (0.166 mM), and  $60.79 \pm 0.1 \mu\text{g/mL}$  (0.218 mM), respectively. According to our results, compounds **11** and **20** had more significant inhibitory effects on MCF-7 and MDA-231 breast cancer cell lines respectively as compared with TAM as a reference drug ( $IC_{50} = 48.35 \pm 0.07 \mu\text{g/mL}$  (0.130 mM) and  $44.69 \pm 1.1 \mu\text{g/mL}$  (0.120 mM), respectively). Moreover, compounds **11** and **20** showed lower cytotoxic effects on WISH normal cells ( $IC_{50} = 116 \pm 1.6 \mu\text{g/mL}$  (0.24 mM) and  $113.6 \pm 1.7 \mu\text{g/mL}$  (0.408 mM), respectively). This means that they are much more effective on cancer proliferative cells without any toxic effects on normal cells. This is in accordance with the results of in silico docking studies for these compounds. In contrast, TAM has high cytotoxicity on normal cells ( $IC_{50} = 30.62 \pm 0.21 \mu\text{g/mL}$  (0.082 mM)). Thus, MCF-7 and MDA-231 were selected for further analysis.

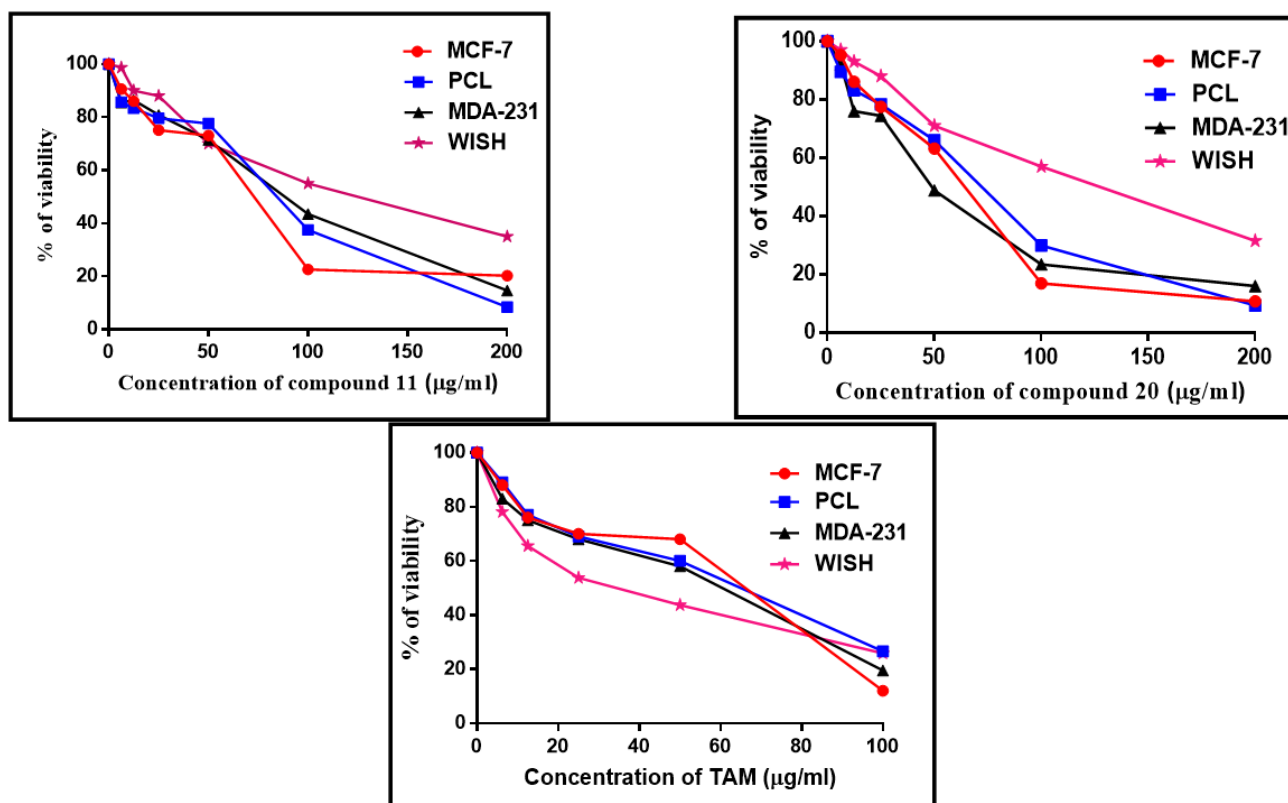


**Figure 3.** Compounds **11** and **20** and tamoxifen inhibit the proliferation of different cancer cell lines. Cells were treated with various concentration of each compound for 48 h and cell viability were plotted against drug concentration to calculate  $IC_{50}$ . The  $IC_{50}$  values of each drug were expressed as mean  $\pm$  SE of three independent experiments performed in triplicates.

### 3.3.2. Detection of Cell Cycle Arrest Phase

Cell cycle arrest phases are the end step that results from the inhibition of mitochondrial complex I and the activation of AMPK protein kinases. Thus, to determine whether the inhibitory effects of compounds **11** and **20** on MCF-7 and MDA cell lines were associated with cell cycle arrest phases, we performed flow cytometry in a dose-dependent manner for each compound ( $1/2 IC_{50}$ ,  $IC_{50}$ ,  $2IC_{50}$ ). In the MCF-7 cell line (compound **11**) and MDA cell line (compound **20**), an increase in the percentage of cells in the sub- $G_0/G_1$  phase was observed in cells at all treated doses compared with the findings in untreated cells. (This is the phase at which cells wait to enter the cell cycle to replicate; when the number of cells in this phase increases, this means that the cell cycle has been arrested and division and replication cannot occur.) The  $1/2 IC_{50}$ ,  $IC_{50}$ , and  $2 IC_{50}$  of compound **11** and compound **20** showed cell cycle arrest at rates of 12.5%, 17.6%, 25.7% and 16.8%, 31.3%, 41.8%, respectively, at sub- $G_0/G_1$  phase compared with untreated MCF-7 cells (5.6%) and MDA-231 cells (10.8%). Therefore, the overall rates of cell cycle arrest in groups treated with compounds **11** and **20** were 87.6%, 82.5%, 74.7% and 83.2%, 68.7%, 58.5%, respectively, compared with untreated MCF-7 cells (94.4%) and MDA-231 cells (89.2%), as illustrated in Figures 4 and 5. Collectively, these results show the improvement in the ability of compounds **11** and **20** to induce the inhibition of mitochondrial complex I, activate adenosine monophosphate-activated protein kinase (AMPK) and cause apoptotic cell death by arresting the cell cycle in sub- $G_0/G_1$  phase in a dose-dependent manner [3].

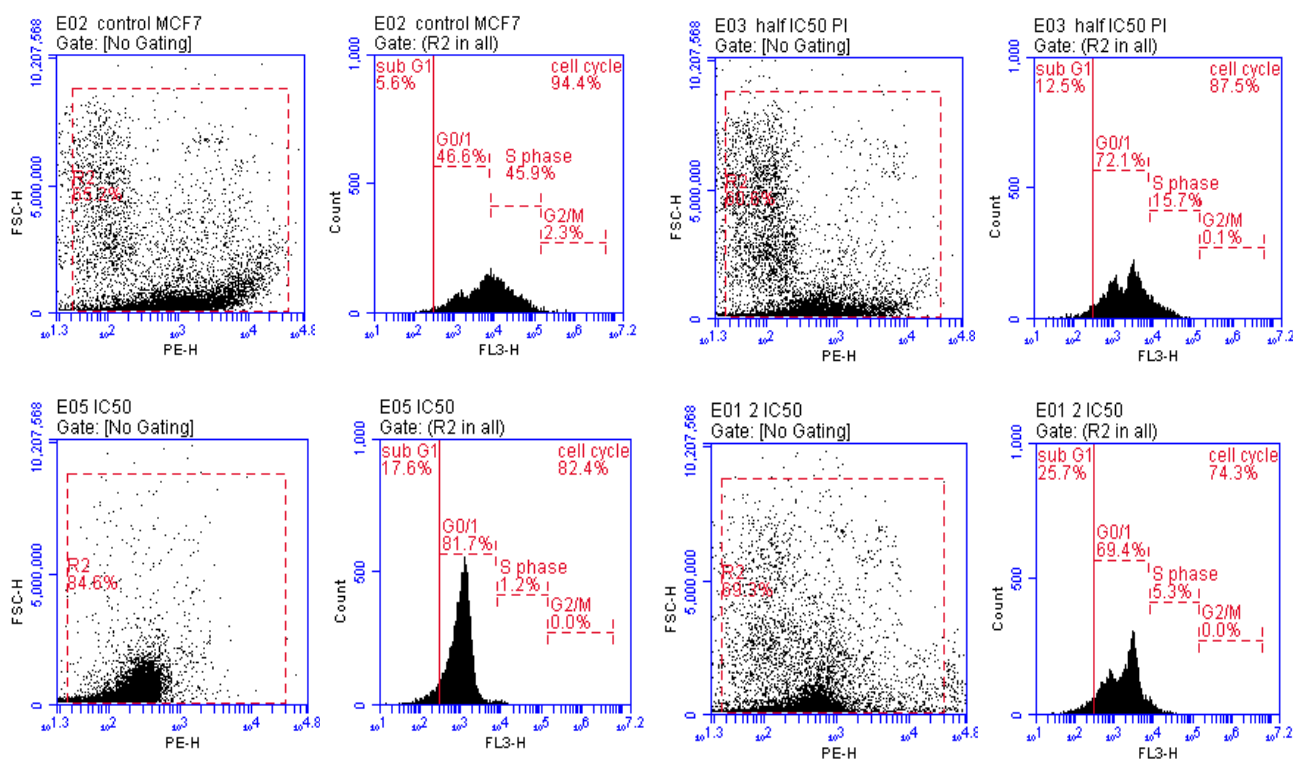


**Figure 4.** Cell cycle phases in MCF-7 cell line (compound **11**) in a dose-dependent manner ( $1/2 IC_{50}$ ,  $IC_{50}$ ,  $2 IC_{50}$ ) after 48 h treatment.

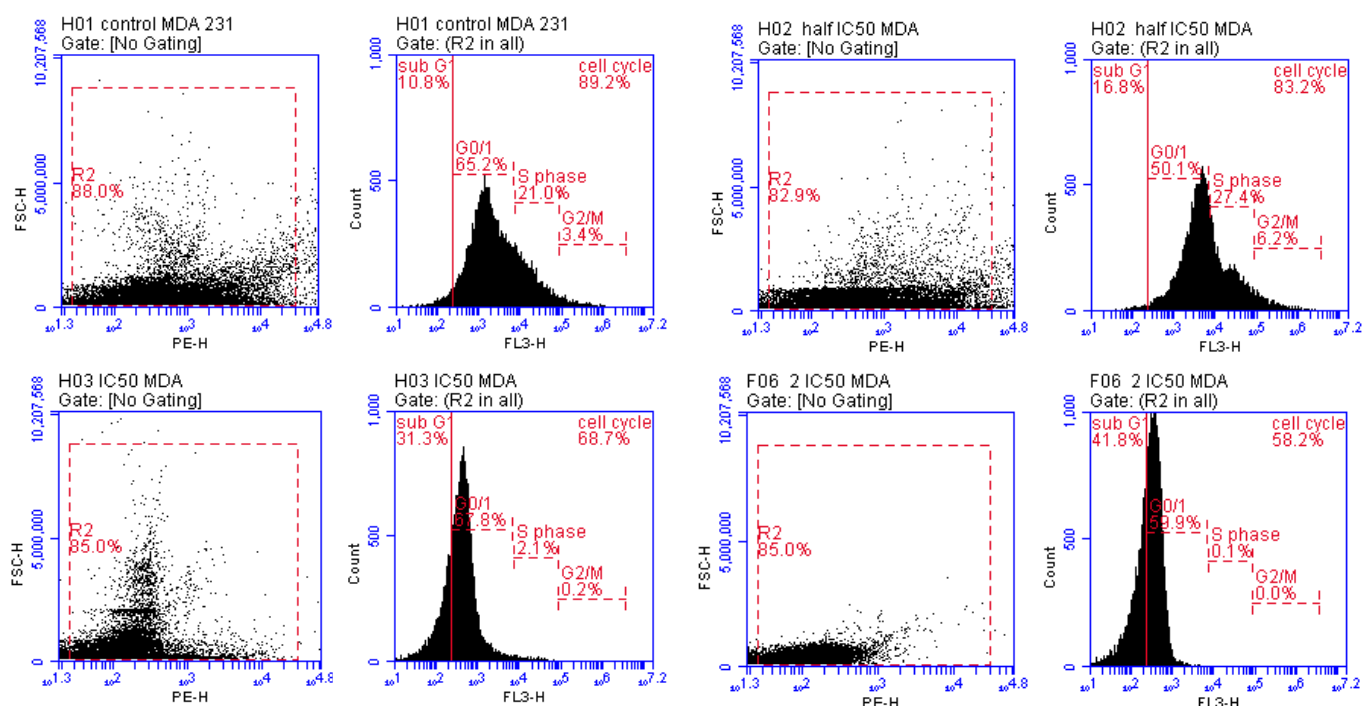


**Figure 5.** Cell cycle phases in MDA-231 cell line (compound 20) in a dose-dependent manner (1/2 IC<sub>50</sub>, IC<sub>50</sub>, 2 IC<sub>50</sub>) after 48 h treatment.

### 3.3.3. Altered mRNA Expression of Apoptosis Markers

The mRNA expression of both MCF-7 and MDA-231 cell lines was quantified by qRT-PCR for Bax, p53 (apoptotic markers), and Bcl-2 (anti-apoptotic marker) genes. Bax and p53 were significantly ( $p < 0.0001$ ) upregulated in cells treated with compounds 11 and 20 in a dose-dependent manner, with maximum expression in the double IC<sub>50</sub> of cells treated with each compound compared with the findings in untreated cells. The Bcl-2 gene was significantly ( $p < 0.0001$ ) downregulated in the cells treated with compounds 11 and 20 in a dose-dependent manner, with minimal expression in the double IC<sub>50</sub> of cells treated with each compound compared with untreated cells, as shown in Figure 6. Thus, the upregulation of Bax and downregulation of Bcl-2 in our results mean that compounds 11 and 20 cause mitochondrial membrane dysfunction, while the upregulation of p53 results from the activation of AMPK. This clarifies the ability of compounds 11 and 20 to inhibit mitochondrial complex I, which is the step that leads to cell cycle arrest and finally induces apoptosis [3,44].

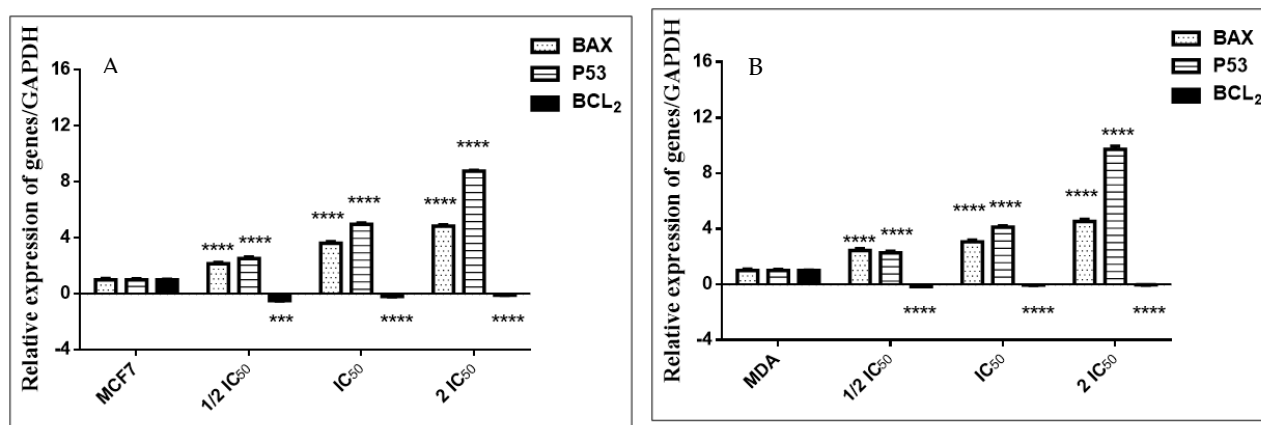


**Figure 6.** (A) Relative expression of Bax, Bcl-2, and p53 in MCF-7 (compound 11) and (B) MDA-231 (compound 20) cell lines in a dose-dependent manner (1/2 IC<sub>50</sub>, IC<sub>50</sub>, 2 IC<sub>50</sub>) after 48 h treatment. Where, different numbers of \*  $p < 0.05$  significant versus the control untreated cells.

### 3.3.4. Inhibition of Warburg Effect through Hexokinase (ELISA)

It is known that cells depend on the continuous intake of glucose for proliferation and survival. This is especially the case for cancer cells, which prefer aerobic glycolysis for ATP production if they are under hypoxic conditions (Warburg effect). The Warburg effect has thus become a novel target for anticancer therapy. Adenosine monophosphate activated protein kinase (AMPK) is a cellular energy receptor that is phosphorylated in response to energy stress (glucose deprivation and decreased cellular ATP/ADP ratios), leading to the inhibition of mTOR that in turn results in the Warburg effect glycolytic pathway to alter this stress and produce ATP. The Warburg effect can be diminished by inhibiting the hexokinase enzyme, the key enzyme for starting glucose consumption in the glycolytic pathway. Our results significantly showed the inhibition of hexokinase activity in MCF-7 (by compound 11) and MDA-231 (by compound 20) cell lines after treatment for 48 h in a dose-dependent manner, as shown in Figure 7. This investigation was performed to confirm their mechanical pathway in stopping cancer proliferation under a decreased level of ATP, which results from the inhibition of mitochondrial complex I [3,45,46].

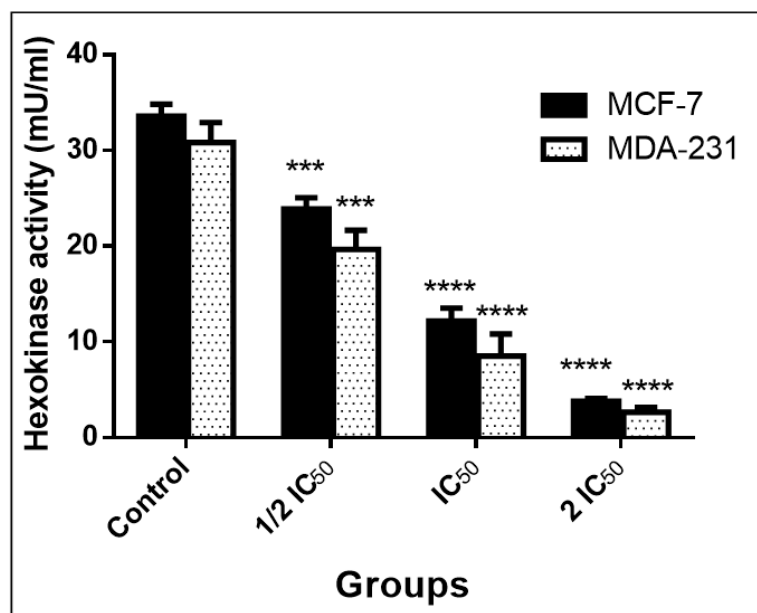


**Figure 7.** Hexokinase inhibitory activity in MCF-7 (compound 11) and MDA-231 (compound 20) cell lines in a dose-dependent manner (1/2 IC<sub>50</sub>, IC<sub>50</sub>, 2 IC<sub>50</sub>) after 48 h treatment. Where, different numbers of \*  $p < 0.05$  significant versus the control untreated cells.

### 3.3.5. Oxidative and Antioxidant Biomarkers

Our results showed a significant increase in the MDA level in MCF-7 cells treated with compound 11 and MDA-231 cells treated with compound 20. On the other hand, our results indicated a significant decrease in the GSH level in MCF-7 cells treated with compound 11 and MDA-231 cells treated with compound 20 in a dose-dependent manner, as shown in Figure 8. This means that compounds 11 and 20 could induce apoptosis in cancer cells by triggering intracellular ROS and inhibiting endogenous antioxidant enzymes. Increased production of ROS in cancer cells leads to the activation of AMPK protein kinase and also causes mitochondrial membrane dysfunction, which finally induces apoptosis and arrests cell survival and proliferation [47–49].

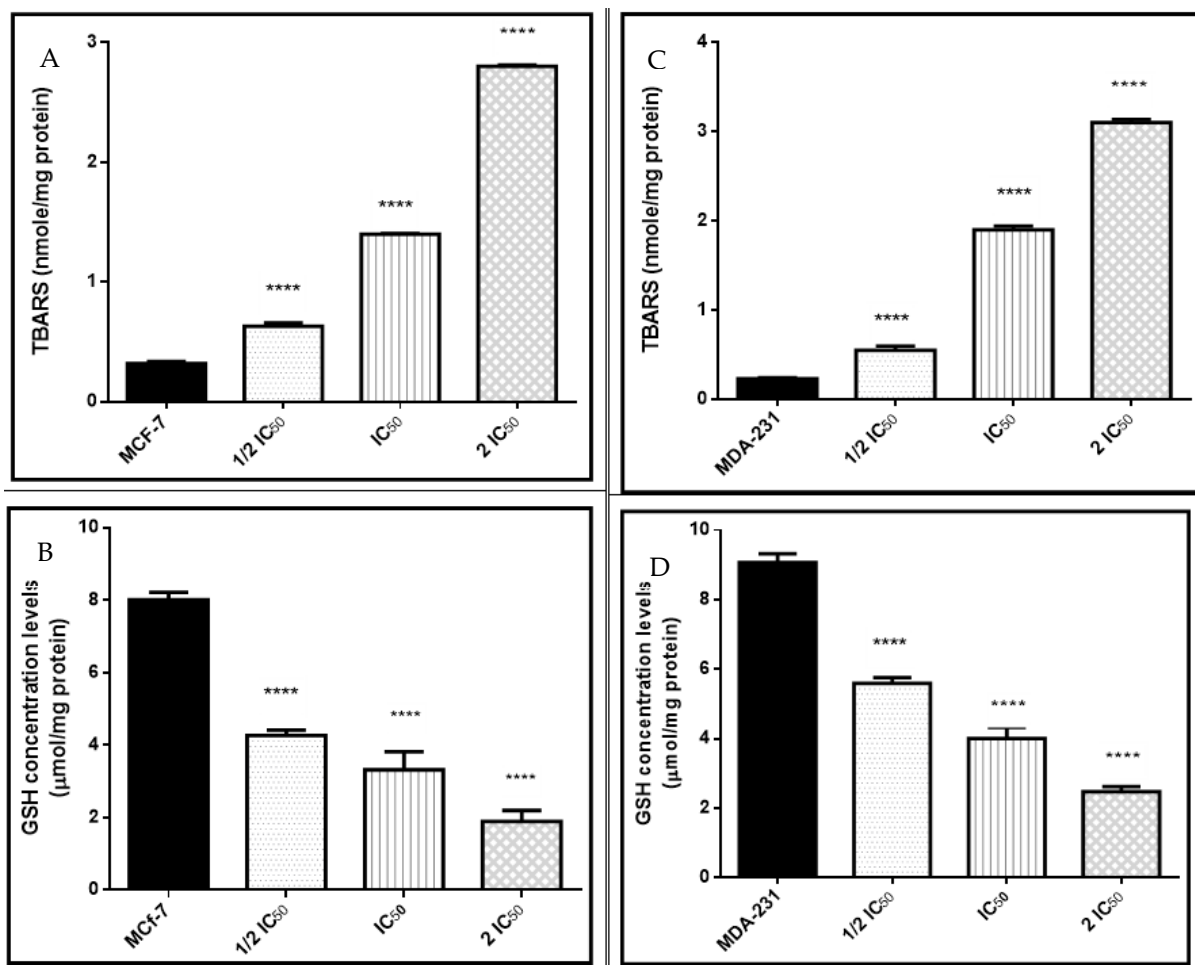


**Figure 8.** (A,B) MDA and GSH levels in MCF-7 (compound **11**) and (C,D) MDA-231 (compound **20**) cell lines in a dose-dependent manner (1/2 IC<sub>50</sub>, IC<sub>50</sub>, 2 IC<sub>50</sub>) after 48 h treatment. Where, different numbers of \*  $p < 0.05$  significant versus the control untreated cells.

### 3.3.6. Immunoblotting Confirms the AMPK/mTOR Pathway

Immunoblotting results showed that compounds **11** and **20** cause a significant increase in AMPK protein kinase folding with a remarkable decrease in mammalian target of rapamycin (mTOR) folding in MCF-7 and MDA-231 breast cancer cell lines in a dose-dependent manner compared with untreated cells, as shown in Figures 9 and 10. These results confirm the mechanical pathways of compounds **11** and **20** to induce apoptosis. The first pathway is that compounds **11** and **20** cause inhibition of mitochondrial complex I, which in turn causes a decrease in ATP production and an increase in the intracellular ROS generation, leading to activation of AMPK through phosphorylation. Once AMPK becomes phosphorylated, it activates P53, leading to cell cycle arrest. It also inactivates mTOR, leading to the Warburg effect, which is also blocked by compounds **11** and **20**. The second pathway involves the ability of compounds **11** and **20** to act on ROS generation, leading to mitochondrial membrane dysfunction and in turn causing an increase in Bax and a decrease in Bcl-2, thereby increasing cytochrome C and caspase 3. These mechanical pathways induce apoptosis and arrest cell survival and proliferation [3,44–49].

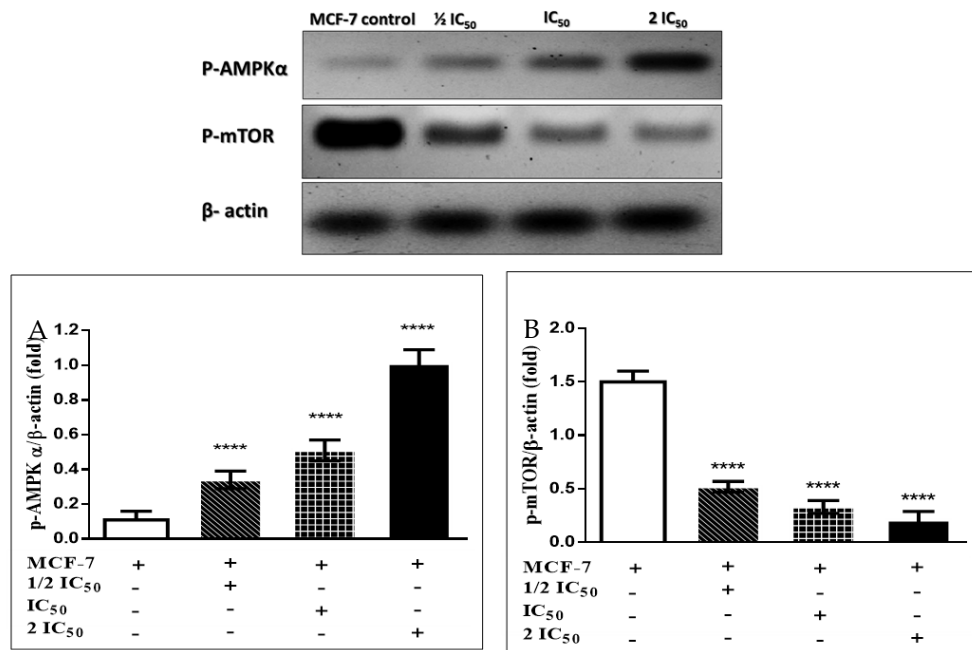


**Figure 9.** Effects of compound 11 on the phosphorylation of AMPK $\alpha$  (A) and mTOR (B) in MCF-7 cells. The cells were treated with the 1/2 IC<sub>50</sub>, IC<sub>50</sub> and 2 IC<sub>50</sub> for 48 h, and the protein phosphorylation levels were relative to  $\beta$ -actin protein (internal control) using western blot analysis. The quantification was determined by Image J software, and the results are presented as mean  $\pm$  S.E. Where, different numbers of \*  $p < 0.05$  significant compared to the untreated control cells.

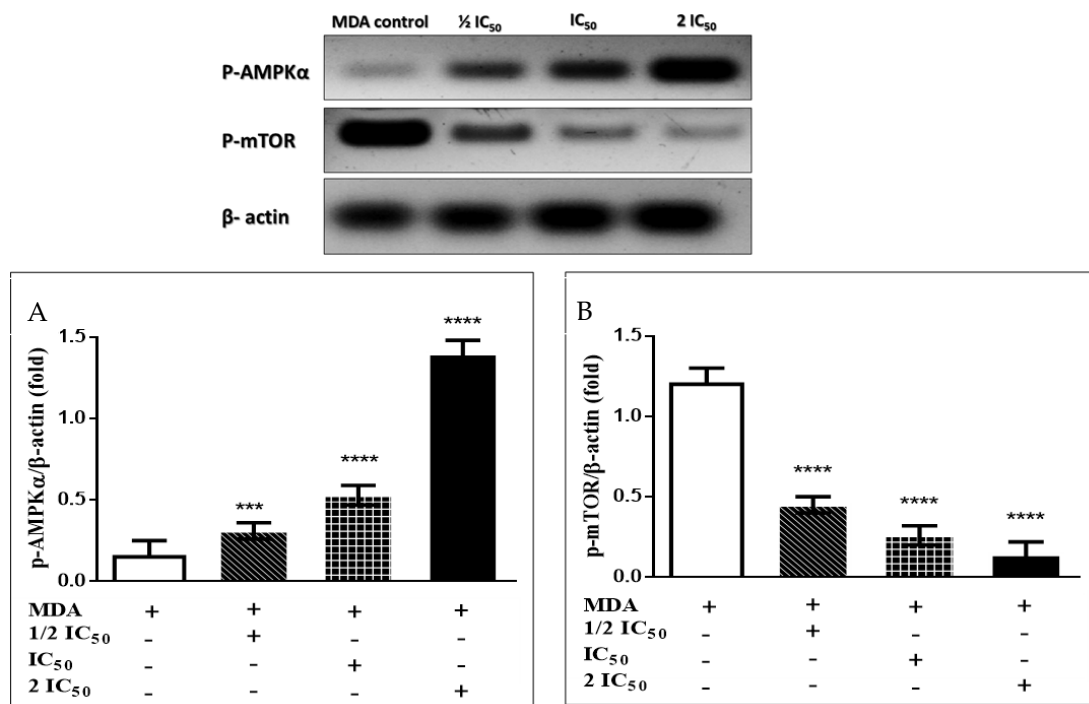


**Figure 10.** Effects of compound 20 on the phosphorylation of AMPK $\alpha$  (A), and mTOR (B) in MDA-231 cells. The cells were treated with the 1/2 IC<sub>50</sub>, IC<sub>50</sub> and 2 IC<sub>50</sub> for 48 h, and the protein phosphorylation levels were relative to  $\beta$ -actin protein (internal control) using western blot analysis. The quantification was determined by Image J software, and the results are presented as mean  $\pm$  S.E. Where, different numbers of \*  $p < 0.05$  significant compared to the untreated control cells.

#### 4. Conclusions

Collectively, as shown in Figure 11, in this study the synthesized compound **11** (quinazoline amino acid Schiff base) and compound **20** (indole amino acid Schiff base) were selected according to their *in silico* molecular binding energy toward NADH oxidoreductase mitochondrial complex I-associated hexokinase, as shown in docking studies. Subsequently, *in vitro* studies confirmed that the selected compounds **11** and **20** can cause apoptosis and cell death through the induction of ROS generation-mediated inhibition of mitochondrial complex I-associated hexokinase. The cellular mechanism by which the interdependence between AMPK activation and mTOR inhibition, p53 activation, and cell cycle arrest blocks the Warburg effect involved in MCF-7 and MDA-231 breast cancer cell lines has been elucidated. Thus, the biological results, as well as the molecular docking studies on compounds **11** and **20**, led us to consider these molecules as promising compounds for future investigation and development of anticancer agents.

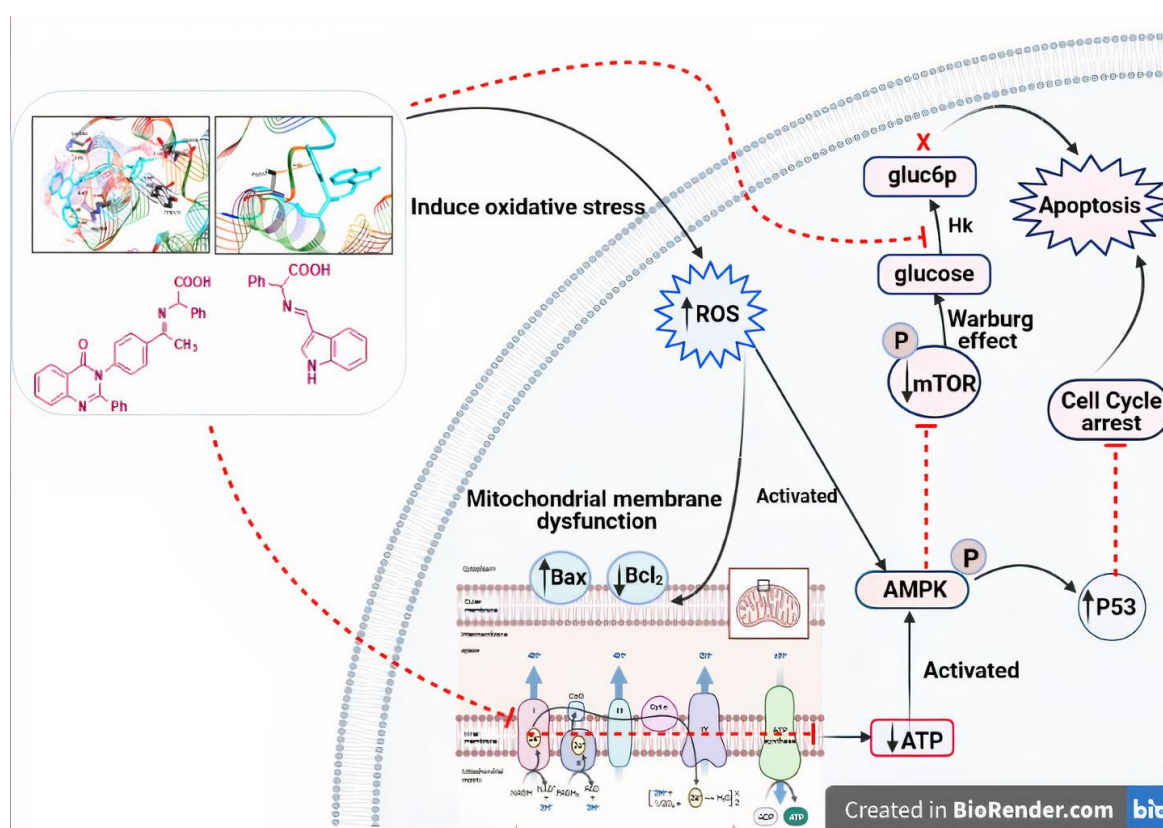


**Figure 11.** Schematic diagram of the signaling pathways involved in compounds **11** and **20** induced mitochondria-associated hexokinase mediated apoptosis.

**Supplementary Materials:** The following are available online.  $^1\text{H}$  and  $^{13}\text{C}$  NMR spectra of the synthesized compounds and the 2D interactions of the other compounds with target proteins.

**Author Contributions:** Conceptualization, A.A.N., A.H.A. and M.M.S.; methodology, A.A.N., A.H.A., M.E.-N. and M.M.S.; software, A.A.N., A.H.A. and M.M.S.; validation, A.A.N., A.H.A., M.E.-N. and M.M.S.; formal analysis, M.E.-N. and M.M.S.; investigation, A.A.N., A.H.A. and M.M.S.; resources, A.A.N., A.H.A. and M.M.S.; data curation, A.A.N., A.H.A. and M.M.S.; writing—original draft preparation, A.A.N., A.H.A. and M.M.S.; writing, review and editing, A.A.N., A.H.A. and M.M.S.; visualization A.A.N., A.H.A. and M.M.S.; supervision, A.A.N., A.H.A. and M.M.S.; project administration, A.A.N., A.H.A. and M.M.S.; funding acquisition, A.A.N., A.H.A., M.E.-N. and M.M.S. All authors have read and agreed to the published version of the manuscript.

**Funding:** This research received no external funding.

**Institutional Review Board Statement:** Not applicable.

**Informed Consent Statement:** Not applicable.

**Data Availability Statement:** Data is contained within the article and the supplementary materials.

**Conflicts of Interest:** The authors declare no conflict of interest.

**Sample Availability:** Samples of the compounds 3 to 20 are available from the authors.

## References

1. von Meyenfeldt, M. Cancer-associated malnutrition: An introduction. *Eur. J. Oncol. Nurs.* **2005**, *9*, 35–38. [[CrossRef](#)]
2. Noser, A.A.; El-Naggar, M.; Donia, T.; Abdelmonsef, A.H. Synthesis, In Silico and In Vitro Assessment of New Quinazolinones as Anticancer Agents via Potential AKT Inhibition. *Molecules* **2020**, *25*, 4780. [[CrossRef](#)]
3. Andrzejewski, S.; Siegel, P.M.; St-Pierre, J. Metabolic profiles associated with metformin efficacy in cancer. *Front. Endocrinol.* **2018**, *9*, 372. [[CrossRef](#)]
4. Andrzejewski, S.; Gravel, S.-P.; Pollak, M.; St-Pierre, J. Metformin directly acts on mitochondria to alter cellular bioenergetics. *Cancer Metab.* **2014**, *2*, 12. [[CrossRef](#)]
5. Andrzejewski, S.; Klimcakova, E.; Johnson, R.M.; Tabariès, S.; Annis, M.G.; McGuirk, S.; Northey, J.J.; Chénard, V.; Sriram, U.; Papadopoli, D.J.; et al. PGC-1 $\alpha$  Promotes Breast Cancer Metastasis and Confers Bioenergetic Flexibility against Metabolic Drugs. *Cell Metab.* **2017**, *26*, 778–787. [[CrossRef](#)] [[PubMed](#)]
6. Owen, M.R.; Doran, E.; Halestrap, A.P. Evidence that metformin exerts its anti-diabetic effects through inhibition of complex 1 of the mitochondrial respiratory chain. *Biochem. J.* **2000**, *348*, 607–614. [[CrossRef](#)]
7. El-Mir, M.Y.; Nogueira, V.; Fontaine, E.; Avéret, N.; Rigoulet, M.; Leverve, X. Dimethylbiguanide inhibits cell respiration via an indirect effect targeted on the respiratory chain complex I. *J. Biol. Chem.* **2000**, *275*, 223–228. [[CrossRef](#)]
8. Griss, T.; Vincent, E.E.; Egnatchik, R.; Chen, J.; Ma, E.H.; Faubert, B.; Viollet, B.; DeBerardinis, R.J.; Jones, R.G. Metformin Antagonizes Cancer Cell Proliferation by Suppressing Mitochondrial-Dependent Biosynthesis. *PLoS Biol.* **2015**, *13*, e1002309. [[CrossRef](#)] [[PubMed](#)]
9. Zhou, G.; Myers, R.; Li, Y.; Chen, Y.; Shen, X.; Fenyk-Melody, J.; Wu, M.; Ventre, J.; Doebber, T.; Fujii, N.; et al. Role of AMP-activated protein kinase in mechanism of metformin action. *J. Clin. Investig.* **2001**, *108*, 1167–1174. [[CrossRef](#)] [[PubMed](#)]
10. Bogachus, L.D.; Turcotte, L.P. Genetic downregulation of AMPK- $\alpha$  isoforms uncovers the mechanism by which metformin decreases FA uptake and oxidation in skeletal muscle cells. *Am. J. Physiol.—Cell Physiol.* **2010**, *299*, 1549–1561. [[CrossRef](#)]
11. Bhat, M.; Yanagiya, A.; Graber, T.; Razumilava, N.; Bronk, S.; Zammit, D.; Zhao, Y.; Zakaria, C.; Metrakos, P.; Pollak, M.; et al. Metformin requires 4E-BPs to induce apoptosis and repress translation of Mcl-1 in hepatocellular carcinoma cells. *Oncotarget* **2017**, *8*, 50542–50556. [[CrossRef](#)]
12. Takahashi, A.; Kimura, F.; Yamanaka, A.; Takebayashi, A.; Kita, N.; Takahashi, K.; Murakami, T. Metformin impairs growth of endometrial cancer cells via cell cycle arrest and concomitant autophagy and apoptosis. *Cancer Cell Int.* **2014**, *14*, 53. [[CrossRef](#)] [[PubMed](#)]
13. Rojas-Ortiz, J.J.; Contreras-Celedón, C.; Gómez-Hurtado, M.A.; Chacón-García, L.; Cortes-García, C.J. Synthesis of Novel Schiff Base Derivates Containing a Fragment of the HIV Integrase Inhibitor Drug Raltegravir. *Proceedings* **2019**, *41*, 5. [[CrossRef](#)]
14. Kajal, A.; Bala, S.; Kamboj, S.; Sharma, N.; Saini, V. Schiff Bases: A Versatile Pharmacophore. *J. Catal.* **2013**, *2013*, 893512. [[CrossRef](#)]
15. Rakesh, K.P.; Darshini, N.; Shubhavathi, T.; Mallesha, N. Biological Applications of Quinazolinone Analogues: A Review. *Org. Med. Chem Int. J.* **2017**, *2*, 555585.
16. Mungroo, M.R.; Shahbaz, M.S.; Anwar, A.; Saad, S.M.; Khan, K.M.; Khan, N.A.; Siddiqui, R. Aryl Quinazolinone Derivatives as Novel Therapeutic Agents against Brain-Eating Amoebae. *ACS Chem. Neurosci.* **2020**, *11*, 2438–2449. [[CrossRef](#)]
17. Hameed, A.; Al-Rashida, M.; Uroos, M.; Ali, S.A.; Arshia; Ishtiaq, M.; Khan, K.M. Quinazoline and quinazolinone as important medicinal scaffolds: A comparative patent review (2011–2016). *Expert. Opin. Ther. Targets* **2018**, *28*, 281–297. [[CrossRef](#)] [[PubMed](#)]
18. Naim, M.J.; Alam, O.; Alam, J.; Bano, F.; Alam, P. Recent review on indole: A privileged scaffold structure. *Int. J. Pharm. Sci. Res.* **2016**, *7*, 51–62.
19. Chadha, N.; Silakari, O. Indoles as therapeutics of interest in medicinal chemistry: Bird’s eye view. *Eur. J. Med. Chem.* **2017**, *134*, 159–184. [[CrossRef](#)] [[PubMed](#)]
20. Gomha, S.M.; Abdelhady, H.A.; Hassain, D.Z.H.; Abdelmonsef, A.H.; El-Naggar, M.; Elaasser, M.M.; Mahmoud, H.K. Thiazole-Based Thiosemicarbazones: Synthesis, Cytotoxicity Evaluation and Molecular Docking Study. *Drug Des. Devel. Ther.* **2021**, *2021*, 659–677. [[CrossRef](#)]
21. El-Maghraby, A.; Abdelmonsef, A. Synthesis, characterization and Insilico molecular docking studies of novel chromene derivatives as Rab23 inhibitors. *Egypt. J. Chem.* **2019**, *20*, 1341–1358.
22. Dasari, T.; Kondagari, B.; Dulapalli, R.; Abdelmonsef, A.H.; Mukkera, T.; Padmarao, L.S.; Malkhed, V.; Vuruputuri, U. Design of novel lead molecules against RhoG protein as cancer target—a computational study. *J. Biomol. Struct. Dyn.* **2017**, *35*, 3119–3139. [[CrossRef](#)] [[PubMed](#)]
23. Abdelmonsef, A.H.; Dulapalli, R.; Dasari, T.; Padmarao, L.S.; Mukkera, T.; Vuruputuri, U. Identification of Novel Antagonists for Rab38 Protein by Homology Modeling and Virtual Screening. *Comb. Chem. High Throughput Screen.* **2016**, *19*, 875–892. [[CrossRef](#)] [[PubMed](#)]

24. Haredi Abdelmonsef, A. Computer-aided identification of lung cancer inhibitors through homology modeling and virtual screening. *Egypt. J. Med. Hum. Genet.* **2019**, *20*, 6. [[CrossRef](#)]
25. Rashdan, H.R.M.; Abdelmonsef, A.H.; Shehadi, I.A.; Gomha, S.M.; Soliman, A.M.M.; Mahmoud, H.K. Synthesis, Molecular Docking Screening and Anti-Proliferative Potency Evaluation of Some New Imidazo[2,1-b]Thiazole Linked Thiadiazole Conjugates. *Molecules* **2020**, *25*, 4997. [[CrossRef](#)]
26. Rashdan, H.; Shehadi, I.; Abdelmonsef, A.H. Synthesis, Anticancer Evaluation, Computer-Aided Docking Studies, and AD-MET Prediction of 1,2,3-Triazolyl-Pyridine Hybrids as Human Aurora B Kinase Inhibitors. *ACS Omega* **2021**, *6*, 1445–1455. [[CrossRef](#)] [[PubMed](#)]
27. Shehadi, I.A.; Rashdan, H.R.M.; Abdelmonsef, A.H. Homology modeling and virtual screening studies of antigen MLLA-42Protein: Identification of novel drug candidates against leukemia—an in silico approach. *Comput. Math. Methods Med.* **2020**, *2020*, 8196147. [[CrossRef](#)] [[PubMed](#)]
28. Abdelmonsef, A.H.; Mosallam, A.M. Synthesis, in vitro biological evaluation and in silico docking studies of new quinazolin-2,4-dione analogues as possible anticarcinoma agents. *J. Heterocycl. Chem.* **2020**, *25*, 4780.
29. Tiwary, B.K.; Zirmire, R.K.; Pradhan, K.; Nanda, A.K. Innovare academic sciences preparation and spectroscopic characterization of inclusion complex of 2-phenyl-4H-benzo [d][1,3] oxazin-4-one and  $\beta$ -cyclodextrin. *Int. J. Pharm. Pharm. Sci.* **2014**, *6*, 7–10.
30. Patel, H.M.; Noolvi, M.N.; Shirkhedkar, A.A.; Kulkarni, A.D.; Pardeshi, C.V.; Surana, S.J. Anti-convulsant potential of quinazolines. *RSC Adv.* **2016**, *6*, 44435–44455. [[CrossRef](#)]
31. Yorur-Goreci, C.; Demir, Z.; Altaş, N. Green Synthesis of New Amino Acid Schiff Bases and Their Biological Activities. *J. Turkish Chem. Soc. Sect. A Chem.* **2016**, *3*, 15–26. [[CrossRef](#)]
32. Berman, H.M.; Westbrook, J.; Feng, Z.; Gilliland, G.; Bhat, T.N.; Weissig, H.; Shindyalov, I.N.; Bourne, P.E. The protein data bank. *Acta Crystallogr. Sect. D Biol. Crystallogr.* **2002**, *58*, 899–907. [[CrossRef](#)]
33. O’Boyle, N.M.; Banck, M.; James, C.A.; Morley, C.; Vandermeersch, T.; Hutchison, G.R. Open Babel: An Open chemical toolbox. *J. Cheminform.* **2011**, *3*, 33. [[CrossRef](#)]
34. Dallakyan, S.; Olson, A.J. Small-Molecule Library Screening by Docking with PyRx. *Chem. Biol.* **2015**, *1263*, 243–250.
35. Dash, S.K.; Ghosh, T.; Roy, S.; Chattopadhyay, S.; Das, D. Zinc sulfide nanoparticles selectively induce cytotoxic and genotoxic effects on leukemic cells: Involvement of reactive oxygen species and tumor necrosis factor alpha. *J. Appl. Toxicol.* **2014**, *34*, 1130–1144. [[CrossRef](#)] [[PubMed](#)]
36. Darzynkiewicz, Z.; Halicka, H.D.; Zhao, H. Analysis of cellular DNA content by flow and laser scanning cytometry. *Adv. Exp. Med. Biol.* **2010**, *675*, 137–147.
37. Kvastad, L.; Solnestam, B.W.; Johansson, E.; Nygren, E.O.; Laddach, N.; Sahlén, P.; Vickovic, S.; Bendigtsen, S.C.; Aaserud, M.; Floer, L.; et al. Single cell analysis of cancer cells using an improved RT-MLPA method has potential for cancer diagnosis and monitoring. *Sci. Rep.* **2015**, *5*, 16519. [[CrossRef](#)]
38. Livak, K.J.; Schmittgen, T.D. Analysis of relative gene expression data using real-time quantitative PCR and the 2- $\Delta\Delta$ CT method. *Methods* **2001**, *25*, 402–408. [[CrossRef](#)] [[PubMed](#)]
39. Salem, M.M.; Donia, T.; Abu-Khudir, R.; Ramadan, H.; Ali, E.M.M.; Mohamed, T.M. Propolis Potentiates Methotrexate Anticancer Mechanism and Reduces its Toxic Effects. *Nutr. Cancer* **2020**, *72*, 460–480. [[CrossRef](#)]
40. Bradford, M.M. A rapid and sensitive method for the quantitation of microgram quantities of protein utilizing the principle of protein-dye binding. *Anal. Biochem.* **1976**, *72*, 248–254. [[CrossRef](#)]
41. Mruk, D.D.; Cheng, C.Y. Enhanced chemiluminescence (ECL) for routine immunoblotting. *Spermatogenesis* **2011**, *1*, 121–122. [[CrossRef](#)] [[PubMed](#)]
42. El-Naggar, M.; Mohamed, M.E.; Mosallam, A.M.; Salem, W.; Rashdan, H.R.; Abdelmonsef, A.H. Synthesis, Characterization, Antibacterial Activity, and Computer-Aided Design of Novel Quinazolin-2,4-dione Derivatives as Potential Inhibitors Against *Vibrio cholerae*. *Evol. Bioinforma.* **2020**, *16*, 1176934319897596. [[CrossRef](#)] [[PubMed](#)]
43. El-Saghier, A.M.; El-Naggar, M.; Hussein, A.H.M.; El-Adasy, A.-B.A.; Olish, M.; Abdelmonsef, A.H. Eco-Friendly Synthesis, Biological Evaluation, and In Silico Molecular Docking Approach of Some New Quinoline Derivatives as Potential Antioxidant and Antibacterial Agents. *Front. Chem.* **2021**, *9*, 679967. [[CrossRef](#)] [[PubMed](#)]
44. Lu, C.C.; Chiang, J.H.; Tsai, F.J.; Hsu, Y.M.; Juan, Y.N.; Yang, J.S.; Chiu, H.Y. Metformin triggers the intrinsic apoptotic response in human AGS gastric adenocarcinoma cells by activating AMPK and suppressing mTOR/AKT signalling. *Int. J. Oncol.* **2019**, *54*, 1271–1281.
45. Chen, Z.; Zhang, H.; Lu, W.; Huang, P. Role of mitochondria-associated hexokinase II in cancer cell death induced by 3-bromopyruvate. *Biochim. Biophys. Acta—Bioenerg.* **2009**, *1787*, 553–560. [[CrossRef](#)]
46. Shafae, A.; Islamian, J.P.; Zarei, D.; Mohammadi, M.; Nejati-Koshki, K.; Farajollahi, A.; Aghamiri, S.M.R.; Yamchi, M.R.; Baradaran, B.; Jafarabadi, M.A. Induction of apoptosis by a combination of 2-deoxyglucose and metformin in esophageal squamous cell carcinoma by targeting cancer cell metabolism. *Iran. J. Med. Sci.* **2019**, *44*, 99–107.
47. Hasanzadeh, D.; Mahdavi, M.; Dehghan, G.; Charoudeh, H.N. Farnesiferol C induces cell cycle arrest and apoptosis mediated by oxidative stress in MCF-7 cell line. *Toxicol. Reports* **2017**, *4*, 420–426. [[CrossRef](#)]
48. Dias Lopes, N.M.; Marinello, P.C.; Sanches, L.J.; da Silva Brito, W.A.; Lovo-Martins, M.I.; Pinge-Filho, P.; Luiz, R.C.; Cecchini, R.; Cecchini, A.L. Patterns of cell death induced by metformin in human MCF-7 breast cancer cells. *Pathol. Res. Pract.* **2020**, *216*, 153199. [[CrossRef](#)]

- 
49. Fu, S.C.; Liu, J.M.; Lee, K.I.; Tang, F.C.; Fang, K.M.; Yang, C.Y.; Su, C.C.; Chen, H.H.; Hsu, R.J.; Chen, Y.W. Cr(VI) induces ROS-mediated mitochondrial-dependent apoptosis in neuronal cells via the activation of Akt/ERK/AMPK signaling pathway. *Toxicol. Vitr.* **2020**, *65*, 104795. [[CrossRef](#)]